

Branching ratios of mesonic and nonmesonic antikaon absorptions in nuclear medium

Takayasu Sekihara,^{1,*} Junko Yamagata-Sekihara,^{2,*} Daisuke Jido,^{3,4} and Yoshiko Kanada-En'yo⁵

¹*Department of Physics, Tokyo Institute of Technology, Tokyo 152-8551, Japan*

²*Departamento de Física Teórica and IFIC, Centro Mixto Universidad de Valencia-CSIC, Institutos de Investigación de Paterna, Aptdo. 22085, 46071 Valencia, Spain*

³*Yukawa Institute for Theoretical Physics, Kyoto University, Kyoto 606-8502, Japan*

⁴*J-PARC Branch, KEK Theory Center, Institute of Particle and Nuclear Studies, High Energy Accelerator Research Organization (KEK), 203-1, Shirakata, Tokai, Ibaraki, 319-1106, Japan*

⁵*Department of Physics, Kyoto University, Kyoto 606-8502, Japan*

(Dated: March 2, 2013)

The branching ratios of K^- absorption in nuclear matter are theoretically investigated in order to understand the mechanism of K^- absorption into nuclei. For this purpose mesonic and nonmesonic absorption potentials are evaluated as functions of nuclear density, the kaon momentum and energy from one- and two-body K^- self-energy, respectively. By using a chiral unitary approach for the s -wave $\bar{K}N$ amplitude we find that both the mesonic and nonmesonic absorption potentials are dominated by the $\Lambda(1405)$ contributions. The fraction of the mesonic and nonmesonic absorptions are evaluated to be respectively about 70% and 30% at the saturation density almost independently on the kaon momentum. We also observe different behavior of the branching ratios to $\pi^+\Sigma^-$ and $\pi^-\Sigma^+$ channels in mesonic absorption due to the interference between $\Lambda(1405)$ and the $I = 1$ nonresonant background, which is consistent with experimental results. The nonmesonic absorption ratios $[\Lambda p]/[\Sigma^0 p]$ and $[\Lambda n]/[\Sigma^0 n]$ are about unity while $[\Sigma^+ n]/[\Sigma^0 p]$ and $[\Sigma^- p]/[\Sigma^0 n]$ are about two due to the $\Lambda(1405)$ dominance in absorption. Taking into account the kaon momenta and energies, the absorption potentials become weaker due to the downward shift of the initial K^-N two-body energy, but this does not drastically change the nonmesonic fraction. The $\Sigma(1385)$ contribution in the p -wave $\bar{K}N$ amplitude is examined and found to be very small compared to the $\Lambda(1405)$ contribution in slow K^- absorption.

PACS numbers: 13.75.Jz, 21.65.Jk, 36.10.Gv

Keywords: $\bar{K}N$ interactions; Mesonic and nonmesonic decay, kaonic atoms; $\Lambda(1405)$ and $\Sigma(1385)$ doorway; Chiral unitary approach

I. INTRODUCTION

Interaction between antikaon (\bar{K}) and nucleon (N) is one of the most important clues for strangeness nuclear physics. The $\bar{K}N$ interaction in the $I = 0$ channel is strongly attractive at low energies and dynamically generates $\Lambda(1405)$ as a quasi-bound state of $\bar{K}N$, which couples to $\pi\Sigma$ as a decay mode [1] (see also [2]). The attractive interaction between $\bar{K}N$ stimulates recent theoretical studies on \bar{K} few-nucleon systems bound mainly by the strong interaction (kaonic nuclei) [3–10] and further nuclear systems with kaons such as $\bar{K}KN$ [11–14] and $\bar{K}\bar{K}N$ [15]. The $\bar{K}N$ interaction is also related to the in-medium properties of \bar{K} [16–21], which is a key to the kaon behavior in high dense matter [22]. However, at present the low-energy $\bar{K}N$ interaction is not well-understood especially in its subthreshold regions.

An important tool to study the phenomenological \bar{K} -nucleus interaction at low energies including the $\bar{K}N$ interaction is kaonic atoms, which are coulombic bound

states of K^- -nucleus with influence of strong interaction. Kaonic atoms have attracted much attention both experimentally and theoretically, because they provide unique information on strong interaction between nucleus and K^- at zero momentum from their binding energies and decay widths [23, 24]. In earlier works, the branching ratios of K^- -nucleus absorption at rest had been experimentally investigated from the 1960's to the 1970's by using emulsions and bubble chambers with, for example, hydrogen [25, 26], deuterium [27], ^4He [28], and heavier nucleus [29]. As a result, it was found that probability to observe nonpionic final state is as large as 20% per stopped K^- for ^4He and heavier nuclei [29] while it is $\sim 1\%$ for deuterium [27]. The fraction of the nonpionic final state for kaon absorption by ^4He was theoretically studied in Ref. [30]. A detailed analysis of the branching ratios for stopped K^- on ^4He was performed in Ref. [28] and the authors reported, for example, the absorption ratio $R_{+-} \equiv [\pi^-\Sigma^+]/[\pi^+\Sigma^-] = 1.8 \pm 0.5$, which is larger than smaller systems, such as ≈ 0.42 for hydrogen [25, 26] and ≈ 0.85 for deuterium [28]. The ratio R_{+-} is also studied in Ref. [31] for p -shell nuclei and $R_{+-} = 1.2\text{--}1.5$ is obtained. It was theoretically suggested in Refs. [32, 33] that the ratio R_{+-} strongly reflects the in-medium properties of $\Lambda(1405)$. In recent works, the energy shift and width of the $1s$ state in kaonic hydrogen is experimen-

*The present address is Institute of Particle and Nuclear Studies, High Energy Accelerator Research Organization (KEK), 1-1, Oho, Ibaraki 305-0801, Japan.

tally extracted in Refs. [34–38], which are followed by theoretical improvements of the $\bar{K}N$ interaction around and below the threshold in Refs. [39–41]. In Refs. [42–45] theoretical analyses of kaonic atoms data including heavy nuclei are performed with subthreshold in-medium $\bar{K}N$ scattering amplitudes and K^- -nucleus potentials by strong interaction as well as properties of kaonic nuclei are discussed. Searches for kaonic nuclei [46–48] were done in stopped K^- experiments by detecting Λ -nucleus correlations in the final state of stopped K^- absorption reactions, motivated by the deeply bound kaonic nuclei predicted in Ref. [4]. However there is no clear evidence yet and further there are discussions on alternative explanations for the peaks observed in experiments [49–51].

One considerable feature of the K^- -nucleus absorption process at rest is that the energy of the K^-N two-body system in the initial state can go below the threshold due to the off-shellness of the bound nucleon inside the nucleus. This leads to the expectation that the absorption pattern is closely related to the $\bar{K}N$ dynamics below the threshold. Especially there are two hyperon resonances, $\Lambda(1405)$ (Λ^*) and $\Sigma(1385)$ (Σ^*) below the $\bar{K}N$ threshold, hence it is natural to consider that their contributions to the absorption process are important. Since Λ^* strongly couples to the $\bar{K}N$ channel in s wave, Λ^* will play the most important role. Therefore, it is interesting to construct \bar{K} -nucleus interactions from the $\bar{K}N$ interaction including Λ^* and Σ^* and to investigate systematically the branching ratios of the \bar{K} -nucleus systems from viewpoint of the low-energy $\bar{K}N$ interaction in order to understand the mechanism of K^- absorption in experiments.

Motivated by these observations, in this study we theoretically investigate the decay pattern of K^- in nuclear matter as a simplified condition for the kaonic atoms by calculating the imaginary part of the K^- self-energy with $\bar{K}N$ interaction as an input. We employ chiral dynamics within a unitary framework (chiral unitary approach) [52–57] for the $\bar{K}N$ interaction. Here we investigate mesonic and nonmesonic decay by taking into account the most probable contributions, that is, the one- and two-nucleon absorption for the mesonic and nonmesonic decay, respectively. Multi-nucleon interactions for the mesonic decay as well as the more than three-nucleon interactions for the nonmesonic decay will be suppressed when the nuclear density is not so high. In this study we consider the K^- self-energy as a function of the kaon energy and momentum as well as the nuclear density. For bound kaons these energy and momentum are determined self-consistently by the equation of motion with the energy dependent potential, and the energy shift and the momentum distribution should be taken into account especially for deeply bound kaon states as suggested in Refs. [42, 43]. For simplicity, we assume the isospin symmetry and consider the symmetric nuclear matter, $\rho_N = \rho_{\text{proton}} + \rho_{\text{neutron}}$ with $\rho_{\text{proton}} = \rho_{\text{neutron}}$. The extension to the case of the asymmetric matter is straightforward.

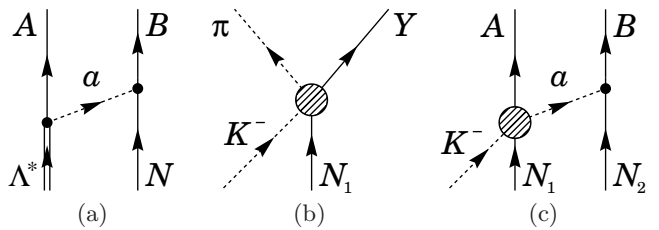


FIG. 1: Feynman diagrams for the decay of \bar{K} -nucleus systems. (a) Λ^* -induced reaction. (b) Mesonic absorption with an explicit K^- in the initial state. (c) Nonmesonic absorption with an explicit K^- in the initial state. In diagrams, A and B denote the baryons in the final state and a denotes the exchange meson.

The present study is a continuation of the study done in Ref. [58]. In Ref. [58] we have discussed nonmesonic decay of Λ^* in a nuclear medium by employing one-meson exchange model as diagrammatically shown in Fig. 1(a), and we have found that the nonmesonic decay ratio $\Gamma_{\Lambda N}/\Gamma_{\Sigma^0 N}$ strongly depends on the Λ^* coupling ratio $g_{\bar{K}N}/g_{\pi\Sigma}$; especially large $g_{\bar{K}N}$ coupling leads to the enhancement of $\Gamma_{\Lambda N}$. Furthermore, by using the chiral unitary approach we have found that $\Gamma_{\Lambda N}/\Gamma_{\Sigma^0 N} \approx 1.2$ almost independently of the nuclear density. In the previous study it has been assumed that one Λ^* is created in nuclear matter and the nonmesonic decay pattern of \bar{K} -nucleus bound systems has been discussed in an idealized condition. In the present study we consider an explicit K^- in the initial state rather than Λ^* as shown in Figs. 1(b) and (c), which enables us to investigate the decay of \bar{K} -nucleus bound systems in more realistic conditions. We discuss how much partition we observe the Λ^* dominance in K^- absorption, which is assumed to be perfect in our previous study. In this work we neglect in-medium effects on mesons, baryons, and hyperon resonances. It is known that the Pauli blocking effect on the nucleons makes Λ^* energy shift above the $\bar{K}N$ threshold as discussed in Refs. [16–19]. Nevertheless, taking into account the in-medium effects on \bar{K} [20] and both on \bar{K} and π [21] as dressed propagators, it was suggested that the in-medium attraction felt by \bar{K} lowers the $\bar{K}N$ threshold and thus Λ^* position moves to the energy close to its free-space value. Although the clear peak of Λ^* would be dissolved in nuclear matter, we use Λ^* without in-medium effects as a zeroth order approximation.

This paper is organized as follows. In Sec. II we explain our formulation for the calculation of the mesonic and nonmesonic absorption potentials for K^- in nuclear matter. We show our results of the absorption potential with s -wave $\bar{K}N \rightarrow MB$ scattering amplitude including the Λ^* contributions in Sec. III. The Σ^* contributions is included in Sec. IV. Section V is devoted to summary of this paper.

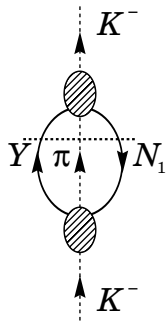


FIG. 2: Feynman diagram for the mesonic K^- absorption processes in nuclear matter. The possible combination of the nucleon (N_1), hyperon (Y), and pion (π) in the intermediate state is given in Table I. The shaded ellipses represent the $K^- N \rightarrow \pi Y$ amplitudes.

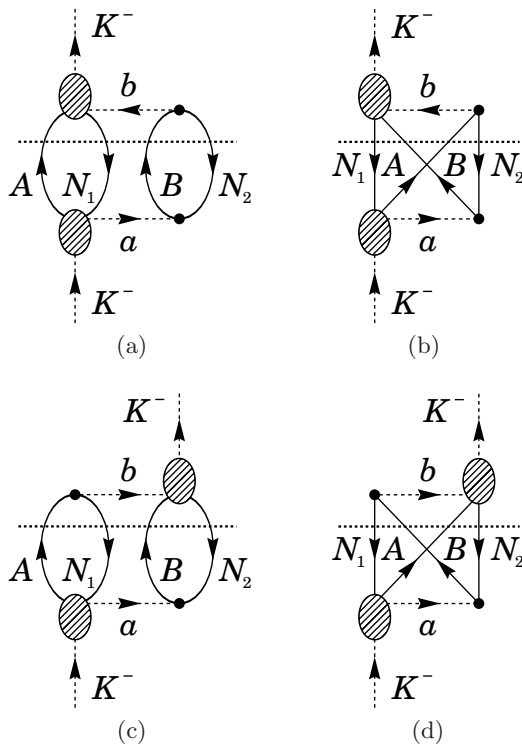


FIG. 3: Feynman diagrams for the nonmesonic K^- absorption processes in nuclear matter. In diagrams, N_1 and N_2 denote nucleons, A and B baryons, and a and b mesons. The shaded ellipses represent the $K^- N \rightarrow MB$ amplitudes.

II. FORMULATION

In this section we formulate the absorption potential of K^- in uniform nuclear matter which is given by the imaginary part of the K^- self-energy in the medium as a function of nuclear density ρ_N as well as the kaon energy E_{K^-} and momentum p_{K^-} . In general, the potential for K^- , V , can be obtained by evaluating the K^- self-energy

U_{K^-} as,

$$2m_{\bar{K}}V = U_{K^-}, \quad (1)$$

with the antikaon mass $m_{\bar{K}}$. The imaginary part of the potential V represents the contribution from K^- absorption,

$$\text{Im}V = \frac{1}{2m_{\bar{K}}} \text{Im}U_{K^-}, \quad (2)$$

in which we are interested here. In evaluation of the imaginary part of the self-energy U_{K^-} we use the Cutkosky rule.

In this study we discuss the mesonic and nonmesonic absorption processes for K^- in nuclear matter as one- and two-body absorption by considering diagrams shown in Figs. 1(b) and (c), respectively. These are the most kinematically probable contributions to K^- absorption. The mesonic absorption potential is evaluated from the self-energy of the Feynman diagram in Fig. 2. For the nonmesonic absorption, on the other hand, we take one-meson exchange model where the Nambu-Goldstone bosons are exchanged between the baryons, as diagrammatically shown in Fig. 3. The sum of the two contributions gives the total K^- self-energy,

$$U_{K^-} = U_{K^-}^{\text{one}} + U_{K^-}^{\text{two}}, \quad (3)$$

where $U_{K^-}^{\text{one}}$ and $U_{K^-}^{\text{two}}$ represent the one- and two-body self-energy, respectively.

The K^- absorption potential is calculated as a function of the nuclear density ρ_N . In our study we describe nuclear matter by using the Thomas-Fermi approximation. In this approximation a bound nucleon with momentum p has energy

$$E_N = M_N + \frac{p^2}{2M_N} + v_N, \quad v_N \equiv -\frac{k_F^2}{2M_N}, \quad (4)$$

where M_N is the nucleon mass and v_N the potential energy for the nucleon with the Fermi momentum $k_F = (3\pi^2\rho_N/2)^{1/3}$. The nucleon momentum p can take a value from 0 to k_F . Since we consider symmetric nuclear matter, we have $k_F(\text{proton}) = k_F(\text{neutron})$. The potential is also a function of the kaon energy and momentum, which are external variables of the self-energy. In contrast, if one considers bound states of a kaon, one has to calculate the Schrödinger or Klein-Gordon equation with this energy-momentum-dependent potential self-consistently. Thus, the potential for the bound kaon should be evaluated with the energy of the bound kaon and the momentum distribution of the bound state. One of the ways to implement the energy and momentum dependence into the potential for the bound state was suggested in Refs. [42, 43].

One important feature of K^- absorption in nuclei is that the center-of-mass energy of the K^-N pair in nuclear matter can go below the threshold value,

TABLE I: Channels of the intermediate states in Fig. 2.

N_1	π	Y
p	π^0	Σ^0
	π^+	Σ^-
	π^-	Σ^+
	π^0	Λ
n	π^-	Λ
	π^-	Σ^0
	π^0	Σ^-

$m_{\bar{K}} + M_N$, due to the off-shellness of the bound nucleon. This can be easily seen by evaluating the center-of-mass energy from the free K^- at rest and bound N momenta, $p_{K^-}^\mu = (m_{\bar{K}}, \mathbf{0})$ and $p_{N_{in}}^\mu = (E_N, \mathbf{p})$; $W = \sqrt{(E_N + m_{\bar{K}})^2 - \mathbf{p}^2} < m_{\bar{K}} + M_N$ because of $E_N \leq M_N$ for the bound nucleon. For a kaon with a finite momentum and a binding energy, the two-body energy W shifts farther downward due to the off-shellness of the kaon. We also note that, since the momentum of the bound nucleon take a value from 0 up to k_F , the span of the K^-N pair energy depends on the density. At certain density around the saturation density, the K^-N energy goes down around the hyperon resonances (Λ^* and Σ^*) sitting below the $\bar{K}N$ threshold. Thus, for these densities, they are expected to give important contributions to the $K^-N \rightarrow MB$ transition amplitudes, which are represented as shaded ellipses in Figs. 2 and 3, and play a crucial role for the absorption pattern.

In order to describe the s -wave $K^-N \rightarrow MB$ transition amplitudes around the $\bar{K}N$ threshold, we use the so-called chiral unitary approach [52–54, 56, 57], which is based on chiral dynamics within a unitary framework. Using the parameter set in Ref. [56], which is fixed by the branching ratios of K^-p at threshold observed with the kaonic hydrogen [25, 26], we can reproduce well the low-energy $\bar{K}N$ scatterings in s wave and dynamically generate the Λ^* resonance. In the chiral unitary approach the Λ^* peak position initiated from the $\bar{K}N$ channel is evaluated to be about 1420 MeV instead of the nominal 1405 MeV [57], which is consistent with the experimental observation [59, 60]. The details of the formulation of the chiral unitary approach used here are given in Ref. [61]. The chiral unitary approach is suitable for our study of K^- absorption since this approach automatically includes the nonresonant background contributions as well as the Λ^* contribution in the scattering amplitude. Here we do not take into account the in-medium effects on the amplitudes determined by the chiral unitary approach. We will also examine the Σ^* contribution in $\bar{K}N$ p -wave in Sec. IV by introducing a simple Breit-Wigner scattering amplitude for Σ^* .

Now let us formulate the K^- potential for the mesonic absorption, which is calculated by considering $K^-N_1 \rightarrow \pi Y$ process for the in-medium nucleon N_1 diagrammatically shown in Fig. 2. In this study we use a symbol $\mu_1 = (\mathbf{p}_1, \chi_1)$ to denote collectively the initial-state nu-

cleon momentum \mathbf{p}_1 and its spin χ_1 , and we assume the isospin symmetry. The cut amplitude for the mesonic process is given as,

$$2\text{Im}U_{K^-}^{\text{one}} = - \int^{k_F} \frac{d^3 p_1}{(2\pi)^3} g_N \overline{\sum_{\lambda}} \sum_{\lambda'} \sum_{(\pi, Y)} \gamma_{\pi Y}(\mu_1; k_F), \quad (5)$$

with the reaction rate for the $K^-N_1 \rightarrow \pi Y$ process,

$$\gamma_{\pi Y}(\mu_1; k_F) \equiv \int d\Phi_{\pi Y} \left| \chi_Y^\dagger \mathcal{T}_{\pi Y} \chi_1 \right|^2 \times (2\pi)^4 \delta^4(p_{K^-} + p_1 - p_\pi - p_Y). \quad (6)$$

Here $g_N = 2$ is the degenerate number of the nucleon for each momentum in nuclear matter (spin up and down), the phase space of the intermediate on-shell state (πY) $d\Phi_{\pi Y}$,

$$d\Phi_{\pi Y} \equiv \frac{d^3 p_\pi}{(2\pi)^3} \frac{1}{2\omega_\pi} \frac{d^3 p_Y}{(2\pi)^3} \frac{2M_Y}{2E_Y}, \quad (7)$$

the $K^-N_1 \rightarrow \pi Y$ scattering amplitude $\mathcal{T}_{\pi Y}$, which is determined by the chiral unitary approach, the Pauli spinor χ_Y for the hyperon, and K^- , π , and hyperon momenta p_{K^-} , p_π , and p_Y , respectively. By means of the two summation symbols with λ and λ' , the sum and average of the scattering amplitude for the polarizations of baryons are done, and (π, Y) under the summation symbol represents the absorption channels to $\pi\Sigma$ and $\pi\Lambda$. Performing the integrations in Eqs. (5) and (6), we obtain,

$$2\text{Im}U_{K^-}^{\text{one}} = - \int_0^{k_F} \frac{dp_1 p_1^2}{\pi^2} \overline{\sum_{\lambda}} \sum_{\lambda'} \sum_{(\pi, Y)} \gamma_{\pi Y}(\mu_1; k_F), \quad (8)$$

$$\gamma_{\pi Y}(\mu_1; k_F) = \frac{p'_{\text{cm}} M_Y}{8\pi^2 W} \int d\Omega_Y \left| \chi_Y^\dagger \mathcal{T}_{\pi Y}(W) \chi_1 \right|^2, \quad (9)$$

with the center-of-mass energy of K^-N_1 system W ,

$$W = \sqrt{(E_1 + E_{K^-})^2 - (\mathbf{p}_1 + \mathbf{p}_{K^-})^2} \quad (10)$$

and the initial nucleon energy E_1 expressed in Eq. (4), and the momentum of the center-of-mass frame for the on-shell πY state p'_{cm} . Here we will take an angular average for the kaon momentum in the integral of the nucleon momentum as

$$W \approx \sqrt{(E_1 + E_{K^-})^2 - (p_1^2 + p_{K^-}^2)}. \quad (11)$$

Next let us consider the nonmesonic absorption process. Taking into account the Feynman diagrams shown in Fig. 3, the cut amplitude for the nonmesonic process can be written as,

$$2\text{Im}U_{K^-}^{\text{two}} = - \int^{k_F} \frac{d^3 p_1}{(2\pi)^3} g_N \int^{k_F} \frac{d^3 p_2}{(2\pi)^3} g_N \times \overline{\sum_{\lambda}} \sum_{\lambda'} \sum_{(Y, N)} \gamma_{YN}(\mu_1, \mu_2; k_F), \quad (12)$$

with the reaction rate for the $K^- NN \rightarrow YN$ process γ_{YN} defined as,

$$\gamma_{YN}(\mu_1, \mu_2; k_F) \equiv \int d\Phi_{YN} |\mathcal{A}_{YN}|^2 \eta_{YN} \times (2\pi)^4 \delta^4(p_{K^-} + p_1 + p_2 - p_Y - p_N), \quad (13)$$

with,

$$d\Phi_{YN} \equiv \frac{d^3 p_Y}{(2\pi)^3} \frac{2M_Y}{2E_Y} \frac{d^3 p_N}{(2\pi)^3} \frac{2M_N}{2E_N}. \quad (14)$$

Here \mathcal{A}_{YN} is the scattering amplitude for the $K^- NN \rightarrow YN$ process, and p_Y and p_N are the hyperon and nucleon momenta in the final state, respectively. The symbol η_{YN} is defined to be,

$$\eta_{YN} = \begin{cases} 2 & \text{for } YN = \Lambda n, \Sigma^0 n, \text{ and } \Sigma^- p, \\ 1 & \text{for others,} \end{cases} \quad (15)$$

in order to take into account the same contribution from initial pn state with exchanged quantum numbers, namely $p(\mu_1)n(\mu_2)$ and $n(\mu_1)p(\mu_2)$ for $K^- pn \rightarrow \Lambda n, \Sigma^0 n$, and $\Sigma^- p$ reactions. The scattering amplitude \mathcal{A}_{YN} can be written by summing all possible channels labeled by i as,

$$\mathcal{A}_{\Lambda p, \Sigma^0 p, \Sigma^+ n} = \frac{1}{\sqrt{2}} \sum_i \xi_i \left[\mathcal{A}_i(K^- p(\mu_1)p(\mu_2) \xrightarrow{a_i} A_i B_i) - \mathcal{A}_i(K^- p(\mu_2)p(\mu_1) \xrightarrow{a_i} A_i B_i) \right], \quad (16)$$

for the $K^- pp \rightarrow \Lambda p, \Sigma^0 p$, and $\Sigma^+ n$ reactions,

$$\mathcal{A}_{\Lambda n, \Sigma^0 n, \Sigma^- p} = \frac{1}{\sqrt{2}} \left[\sum_i \xi_i \mathcal{A}_i(K^- p(\mu_1)n(\mu_2) \xrightarrow{a_i} A_i B_i) - \sum_i \xi_i \mathcal{A}_i(K^- n(\mu_2)p(\mu_1) \xrightarrow{a_i} A_i B_i) \right], \quad (17)$$

for the $K^- pn \rightarrow \Lambda n, \Sigma^0 n$, and $\Sigma^- p$ reactions, and

$$\mathcal{A}_{\Sigma^- n} = \frac{1}{\sqrt{2}} \sum_i \xi_i \left[\mathcal{A}_i(K^- n(\mu_1)n(\mu_2) \xrightarrow{a_i} A_i B_i) - \mathcal{A}_i(K^- n(\mu_2)n(\mu_1) \xrightarrow{a_i} A_i B_i) \right], \quad (18)$$

for the $K^- nn \rightarrow \Sigma^- n$ reaction. Here a_i represents the exchange meson, and A_i and B_i are the baryons in the final state. The explicit channels are given in Table II. The amplitude \mathcal{A} for the $K^- N_1(\mu_1)N_2(\mu_2) \xrightarrow{a} AB$ process is calculated in the one-meson exchange model,

$$\mathcal{A}_i(K^- N_1(\mu_1)N_2(\mu_2) \xrightarrow{a} AB) = \chi_A^\dagger \mathcal{T}_{aA}(W) \chi_1 \times \tilde{\Pi}_a(q_a^2) \times \tilde{V}_{aN_2 B} \chi_B^\dagger \mathbf{q}_a \cdot \boldsymbol{\sigma} \chi_2, \quad (19)$$

TABLE II: Possible channels for Eqs. (16)–(18). Here N_1 and N_2 are the nucleons in the initial state, a is the exchange meson, and A and B are the baryons in the final state. ξ is the relative sign of the amplitude coming from the exchange of the final state baryons, and α and β are the Clebsch-Gordan coefficients for the MBB coupling.

N_1	N_2	a	A	B	ξ	α	β
p	p	K^-	p	Λ	+	$-2/\sqrt{3}$	$1/\sqrt{3}$
		η	Λ	p	–	$1/\sqrt{3}$	$-2/\sqrt{3}$
		π^0	Λ	p	–	1	0
p	p	K^-	p	Σ^0	+	0	1
		π^0	Σ^0	p	–	1	0
		η	Σ^0	p	–	$1/\sqrt{3}$	$-2/\sqrt{3}$
p	p	\bar{K}^0	n	Σ^+	+	0	$\sqrt{2}$
		π^-	Σ^+	n	–	$\sqrt{2}$	0
p	n	\bar{K}^0	n	Λ	+	$-2/\sqrt{3}$	$1/\sqrt{3}$
		η	Λ	n	–	$1/\sqrt{3}$	$-2/\sqrt{3}$
		π^0	Λ	n	–	–1	0
n	p	K^-	n	Λ	+	$-2/\sqrt{3}$	$1/\sqrt{3}$
		π^-	Λ	n	–	$\sqrt{2}$	0
p	n	\bar{K}^0	n	Σ^0	+	0	–1
		π^0	Σ^0	n	–	–1	0
		η	Σ^0	n	–	$1/\sqrt{3}$	$-2/\sqrt{3}$
n	p	K^-	n	Σ^0	+	0	1
		π^-	Σ^0	n	–	$\sqrt{2}$	0
p	n	K^-	p	Σ^-	+	0	$\sqrt{2}$
		π^+	Σ^-	p	–	$\sqrt{2}$	0
		π^0	Σ^-	p	–	1	0
n	p	η	Σ^-	p	–	$1/\sqrt{3}$	$-2/\sqrt{3}$
n	n	K^-	n	Σ^-	+	0	$\sqrt{2}$
		π^0	Σ^-	n	–	–1	0
		η	Σ^-	n	–	$1/\sqrt{3}$	$-2/\sqrt{3}$

where the symbol ξ denotes the relative sign of the amplitude coming from the exchange of the final-state baryons. In the amplitude \mathcal{A}_i , $\mathcal{T}_{aA}(W)$ is the $K^- N_1 \rightarrow aA$ scattering amplitude, which is determined by the chiral unitary approach, with the energy W expressed in Eq. (11). The meson propagator $\tilde{\Pi}_a$ with the meson momentum $q^\mu = p_B^\mu - p_2^\mu$ includes the short-range correlations [62],

$$\tilde{\Pi}_a(q^2) = \left(\frac{\Lambda^2}{\Lambda^2 - q^2} \right)^2 \frac{1}{q^2 - m_a^2} - \left(\frac{\Lambda^2}{\Lambda^2 - \tilde{q}^2} \right)^2 \frac{1}{\tilde{q}^2 - m_a^2}, \quad (20)$$

with $\tilde{q}^2 = q^2 - q_C^2$, where we choose typical parameter set, $\Lambda = 1.0$ GeV and $q_C = 780$ MeV [63]. The coefficient of the meson-baryon-baryon coupling $\tilde{V}_{aN_2 B}$ is determined by the flavor SU(3) symmetry as,

$$\tilde{V}_{aN_2 B} = \alpha_{aN_2 B} \frac{D+F}{2f} + \beta_{aN_2 B} \frac{D-F}{2f}, \quad (21)$$

with empirical values of $D+F = 1.26$ and $D-F = 0.33$, which reproduce the hyperon β decays observed in experiments, and $f = f_\pi = 93.0$ MeV commonly for all the mesons. The SU(3) Clebsch-Gordan coefficients α and β

are listed in Table II. The $K^- N_1 \rightarrow aA$ scattering amplitude \mathcal{T}_{aA} has the indices of spinors for N_1 (χ_1) and A (χ_A), whereas the Pauli matrices σ^i ($i = 1, 2, 3$) appearing in Eq. (19) are given in the space of the spinors for N_2 (χ_2) and B (χ_B). We emphasize that the antisymmetric combinations for initial nucleons are realized as, *e.g.*, $(|p(\mu_1)p(\mu_2)\rangle - |p(\mu_2)p(\mu_1)\rangle)/\sqrt{2}$ in the amplitudes $\mathcal{A}_{\Lambda p, \Sigma^0 p, \Sigma^+ n}$ [see Eqs. (16)–(18) and Table II].

Performing the integrations in Eqs. (12) and (13), we obtain,

$$2\text{Im}U_{K^-}^{\text{two}} = - \int_0^{k_F} \frac{dp_1 p_1^2}{\pi^2} \int_0^{k_F} \frac{dp_2 p_2^2}{\pi^2} \int_{-1}^1 \frac{d\cos\theta_{12}}{2} \times \sum_{\lambda} \sum_{\lambda'} \sum_{(Y,N)} \gamma_{YN}(\mu_1, \mu_2; k_F), \quad (22)$$

$$\gamma_{YN}(\mu_1, \mu_2; k_F) = \frac{p_{\text{cm}}'' M_Y M_N}{4\pi^2 E_{\text{tot}}} \int d\Omega_N |\mathcal{A}_{YN}|^2 \eta_{YN}, \quad (23)$$

with momentum p_{cm}'' for the on-shell Y and N states in the center-of-mass frame and total energy $E_{\text{tot}} = \sqrt{(p_Y + p_N)^2}$.

III. RESULTS

We now show our results for the K^- absorption potential as a function of nuclear density ρ_N . First we consider the self-energy of kaon at rest in nuclear matter with $p_{K^-}^\mu = (m_K, \mathbf{0})$. Next we see the absorption widths for kaons with finite momenta and energies in Sec. III D. In this section we concentrate on contributions from the s -wave $\bar{K}N$ interaction in the K^- absorption reaction, because, as we have already mentioned, the resonance $\Lambda(1405)$ (Λ^*) just below the $\bar{K}N$ threshold in s wave will play the most important role in the K^- absorption process. Later we will discuss the $\Sigma(1385)$ contributions in Sec. IV.

First of all, let us recall that the energy of a two-body system of the kaon at rest and a nucleon inside the nucleus can be less than the $\bar{K}N$ threshold energy owing to the off-shellness of the bound nucleons. The accessible energy range depends on the Fermi momentum for the nucleons, namely the nuclear density, as shown in Eq. (4). The relation between the accessible energy range and the nuclear density is shown in Fig. 4(a). As one can see from Fig. 4(a), $\bar{K}N$ two body systems can have lower energies in higher densities and vice versa. Oppositely, there is a range of density in which a fixed value W can be achieved by the energy of K^-N , as shown in Fig. 4(a). This means that strength of the Λ^* contribution to the $K^-p \rightarrow MB$ transitions in absorption reactions depends on the nuclear density. Hence, in order to see in which density Λ^* appears in the absorption reaction, we show the absolute values of the scattering amplitude for the $K^-p \rightarrow (\pi\Sigma)^0$ and $\pi^0\Lambda$ transitions in Fig. 4(b). From

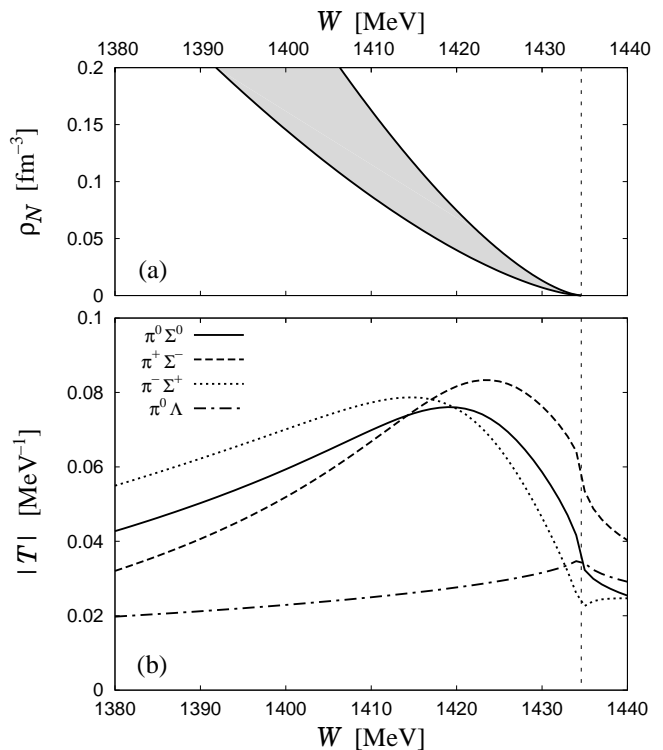


FIG. 4: Range of energy which can be achieved by a fixed energy W of the K^- at rest and a bound nucleon in the nucleus [the shaded area of (a)]. We also show absolute values of the scattering amplitude $|T|$ for the $K^-p \rightarrow (\pi\Sigma)^0$ and $\pi^0\Lambda$ transitions as functions of the energy of the K^-p system, W (b). The vertical lines represent the $\bar{K}N$ threshold.

Fig. 4 we can see that the Λ^* spectra in the $(\pi\Sigma)^0$ channels have a peak around 1420 MeV with a 40 MeV width, which energy can be achieved by a pair of K^-p in nuclear matter with the density $\rho_N \approx 0.05\text{--}0.1 \text{ fm}^{-3}$. We also see that at the saturation density $\rho_0 = 0.17 \text{ fm}^{-3}$ the energy of the K^-p pair is around 1400 MeV, which is in the Λ^* resonance peak. Owing to the presence of the Λ^* resonance, the amplitudes have strong energy dependence. This will make nontrivial ρ_N dependence to mesonic and nonmesonic absorption potentials.

It is also important noting that the peak structure in the $(\pi\Sigma)^0$ amplitude comes from Λ^* with $I = 0$ but the peak position is slightly different in each charged channel. This is because the $I = 1$ nonresonant contributions are not so small and the interference between the $I = 0$ and $I = 1$ contributes in the opposite way for the $\pi^\pm\Sigma^\mp$ channels.

A. Mesonic absorption

First we consider the mesonic absorption potential of K^- . We note that in mesonic absorption $K^-p \rightarrow (\pi\Sigma)^0$ processes contain the Λ^* resonance whereas $K^-p \rightarrow \pi^0\Lambda$ and $K^-n \rightarrow (\pi Y)^-$ processes do not have the Λ^* contri-

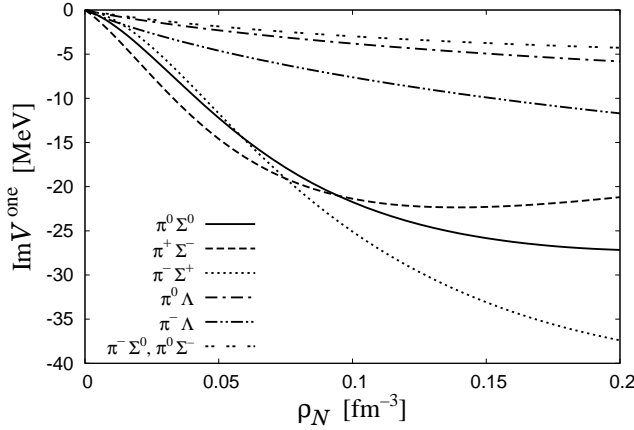


FIG. 5: Mesonic absorption potential ($\text{Im}V^{\text{one}}$) for K^- at rest in nuclear matter as a function of nuclear density. The potentials for $K^- n \rightarrow \pi^- \Sigma^0$ and $\pi^0 \Sigma^-$ have the same values owing to the isospin symmetry.

butions. We also note that we expect that the mesonic absorption potential would be proportional to ρ_N , if the $\bar{K}N$ amplitude would not depend on energy.

In Fig. 5, we show the result of the mesonic absorption potential of K^- at rest in nuclear matter. From the figure, we find that absorption to the $(\pi\Sigma)^0$ states are dominant to the other channels. Since the Λ^* resonance appears selectively in the $K^- p \rightarrow (\pi\Sigma)^0$ transitions, this result shows that the Λ^* contribution is indeed important for the mesonic absorption of K^- in these densities, and that K^- at rest is absorbed through the Λ^* resonance (Λ^* doorway process). Thus, if one observes large branching ratios of $(\pi\Sigma)^0$ in K^- absorption into nuclei, this observation indicates that the Λ^* doorway process dominates the K^- absorption reaction. As for the density dependence of the mesonic absorption potential, the potential for the $(\pi\Sigma)^0$ channels do not show ρ_N^1 -like dependence around $\rho_N > 0.1 \text{ fm}^{-3} \approx 0.6\rho_0$ whereas that for the $\pi^0\Lambda$, $\pi^-\Lambda$, and $(\pi\Sigma)^-$ states shows ρ_N^1 dependence. This is owing to the energy dependence of the $\bar{K}N$ amplitude coming from the Λ^* resonance.

The total sum of the mesonic absorption potential is shown in Fig. 6 as a function of nuclear density. The total value of the mesonic absorption width ($= -2\text{Im}V^{\text{one}}$) amounts to about 200 MeV at the saturation density ($\rho_0 = 0.17 \text{ fm}^{-3}$). The large value of the absorption width is caused because, in addition to that the K^-p energy in the realistic nuclear density is within the range of the Λ^* peak, the number of the initial-state nucleons which can create Λ^* becomes large as the nuclear density increases, as seen in Eq. (8). Here we note that moderate absorption width will be obtained when in-medium $\bar{K}N$ scattering amplitude rather than the free space is used.

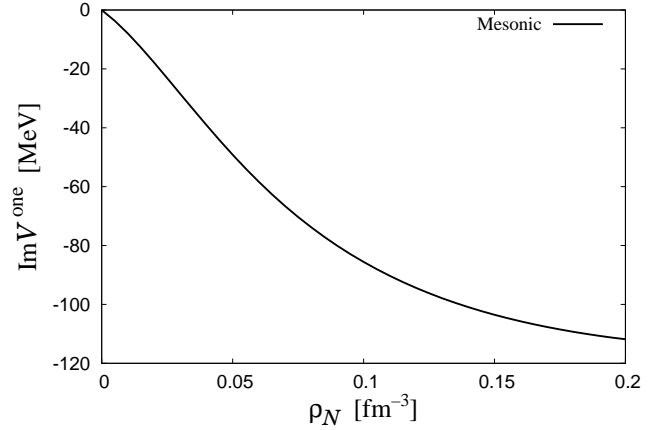


FIG. 6: Total sum of mesonic absorption potential ($\text{Im}V^{\text{one}}$) for K^- at rest in nuclear matter as a function of nuclear density.

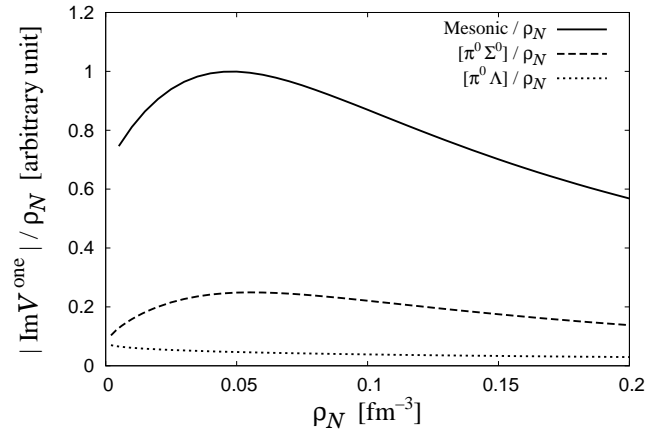


FIG. 7: Absolute absorption potentials divided by ρ_N for total, $\pi^0\Sigma^0$, and $\pi^0\Lambda$ contributions as functions of nuclear density in arbitrary unit.

Indeed, by using an approximation,

$$\sum_{(\pi, Y)} \frac{p'_{\text{cm}} M_Y}{8\pi^2 W} \int d\Omega_Y |\mathcal{T}_{\pi Y}^{\text{med}}(W; \rho)| \approx -2\text{Im}T_{K^-p}^{\text{med}}(W; \rho), \quad (24)$$

for the in-medium $K^-N \rightarrow MB$ scattering amplitude $T_{MB}^{\text{med}}(W; \rho)$ and taking value of $\text{Im}T_{K^-p}^{\text{med}}(W; \rho)$ from Ref. [21], we roughly estimate the mesonic absorption potential with the in-medium amplitude to be $\text{Im}V^{\text{one}} \sim -40 \text{ MeV}$ at the saturation density ρ_0 . The obtained value is about two-fifths of our results (see Fig. 6) and consistent with these preceding works [21, 43], in which in-medium scattering amplitudes are employed to calculate the absorption potential. The total mesonic absorption potential shows non- ρ_N^1 dependence because of the Λ^* doorway contributions. In order to see at which density the Λ^* contribution is large, we plot in Fig. 7 the absolute absorption potentials divided by the nuclear den-

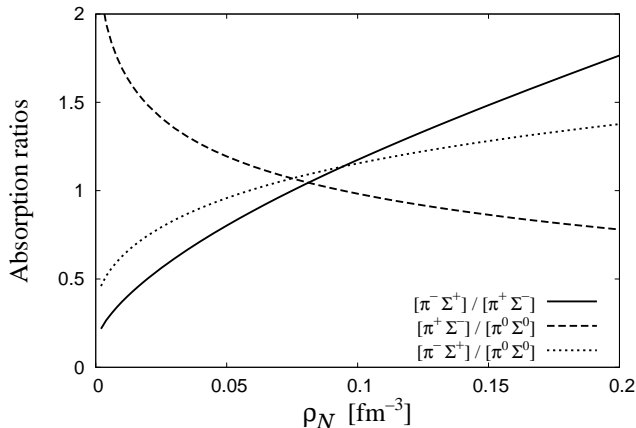


FIG. 8: Ratios of mesonic absorption potentials for $[\pi^-\Sigma^+]/[\pi^+\Sigma^-]$, $[\pi^+\Sigma^-]/[\pi^0\Sigma^0]$, and $[\pi^-\Sigma^+]/[\pi^0\Sigma^0]$ as functions of nuclear density.

sity, $|\text{Im}V^{\text{one}}|/\rho_N$, for the total and the $\pi^0\Sigma^0$ and $\pi^0\Lambda$ mesonic channels as functions of the nuclear density. As one can see from Eqs. (8) and (9), $|\text{Im}V^{\text{one}}|/\rho_N$ takes value approximately proportional to the squared scattering amplitude $|\mathcal{T}_{\pi Y}|^2$ with energies achieved by the considering nuclear density [see also Fig. 4(a)]. Therefore, $|\text{Im}V^{\text{one}}|/\rho_N$ reflects the structure of the $K^-N \rightarrow \pi Y$ transition process. From Fig. 7, there is no structure in the potential for the $\pi^0\Lambda$ channel divided by ρ_N , because the $K^-p \rightarrow \pi^0\Lambda$ process does not have the Λ^* contribution. On the other hand, a local maximum appears at $\rho_N \approx 0.05 \text{ fm}^{-3} \approx 0.3\rho_0$ in case of the total as well as the $\pi^0\Sigma^0$ channel, which indicates enhancement of absorption, due to the Λ^* doorway contribution. The position of the maximum reflects the matching condition of K^-p energy W to the Λ^* peak position via the Λ^* resonance contribution. The fact that a local maximum of $|\text{Im}V^{\text{one}}|/\rho_N$ appears at $\rho_N \approx 0.05 \text{ fm}^{-3} \approx 0.3\rho_0$ is expected from Fig. 4, which shows that this nuclear density corresponds to the peak position of Λ^* in K^-p energy $W \approx 1420 \text{ MeV}$.

Another interesting feature of the absorption potential shown in Fig. 5 is that the behavior of the absorption to the $\pi^0\Sigma^0$, $\pi^+\Sigma^-$, and $\pi^-\Sigma^+$ channels is different from each other, especially at higher densities ($\gtrsim 0.1 \text{ fm}^{-3} \approx 0.6\rho_0$). This comes from the slight difference of the Λ^* spectrum in each channel stemming from the interference between Λ^* in $I = 0$ and the $I = 1$ nonresonant background as shown in Fig. 4(b). At the saturation density the K^-p energy achieves $\approx 1400 \text{ MeV}$, where the squared amplitude $|\mathcal{T}_{\pi^-\Sigma^+}|^2$ is about two times larger than $|\mathcal{T}_{\pi^+\Sigma^-}|^2$ (see Fig. 4), hence the absorption to the $\pi^-\Sigma^+$ channel becomes about two times larger than the $\pi^+\Sigma^-$ channel.

Even though the Λ^* resonance sits in the $I = 0$ channel, the interference between the $I = 0$ and $I = 1$ contributions makes the peak position of the Λ^* spectrum shift in the opposite direction in the $\pi^\pm\Sigma^\mp$ channels as

seen in Fig. 4. The effect of the peak shift can be clearly seen in the density dependence of the ratios of K^- absorption into $(\pi\Sigma)^0$ channels, because the density determines the accessible energy of the two-body system of K^- and a bound nucleon. In Fig. 8 we plot the ratios of the mesonic absorption potential for the $\pi^0\Sigma^0$, $\pi^+\Sigma^-$, and $\pi^-\Sigma^+$ channels. As one can see, while the ratio $[\pi^-\Sigma^+]/[\pi^+\Sigma^-]$, which we denote R_{+-} , is less than unity in $\rho_N < 0.08 \text{ fm}^{-3} \approx 0.5\rho_0$, it gets larger as the density increases and becomes ~ 1.6 at the saturation density. This tendency comes from the facts that the upward shift of the Λ^* peak is seen in the $K^-p \rightarrow \pi^+\Sigma^-$ amplitude while the downward shift in $K^-p \rightarrow \pi^-\Sigma^+$ and that the smaller Fermi momentum for the nucleon, or the lower density, probes the Λ^* spectrum in energies closer to the threshold, while the higher density probes the lower energy of the Λ^* spectrum. We also show the ratios of the mesonic absorption potentials for $[\pi^\pm\Sigma^\mp]/[\pi^0\Sigma^0]$ in Fig. 8. Here we note that the $\pi^0\Sigma^0$ channel has no $I = 1$ contribution and can be a guide for the Λ^* spectrum. The ratio $[\pi^\pm\Sigma^\mp]/[\pi^0\Sigma^0]$ shows opposite behaviors to each other; $[\pi^+\Sigma^-]/[\pi^0\Sigma^0]$ ($[\pi^-\Sigma^+]/[\pi^0\Sigma^0]$) becomes weaker (large) as the density increases. All of the three ratios in Fig. 8 is almost unity at $\rho_N \approx 0.08 \text{ fm}^{-3} \approx 0.5\rho_0$.

The increase of the absorption ratio R_{+-} as the density increases also indicates the nature of the Λ^* resonance. As mentioned before, the increase of the ratio means that the Λ^* peak is shifted upward in the $\pi^+\Sigma^-$ channel and downward in the $\pi^-\Sigma^+$ channel, which is a consequence of the interference of $I = 0$ and $I = 1$ and is determined by the relative sign of the $I = 0$ and $I = 1$ amplitudes. Then, an important point is that the inversion of the $\pi^+\Sigma^-$ dominance to the $\pi^-\Sigma^+$ dominance takes place at relatively lower density $\rho_N \approx 0.08 \text{ fm}^{-3} \approx 0.5\rho_0$. This means that the peak position of the Λ^* spectrum in $K^-p \rightarrow (\pi\Sigma)^0$ should be at an energy closed to the $\bar{K}N$ threshold rather than at 1405 MeV , because lower densities cannot probe the energy far from the threshold. In fact, we have an experimental indication of the ratio increase and the inversion of the dominance channel. Namely, while the ratio R_{+-} is 0.42 for kaonic hydrogen [25, 26], which constrains the ratio at the zero density, it becomes 0.85 for kaonic deuterium, 1.8 ± 0.5 for kaonic ^4He [28], and 1.2 – 1.5 for p -shell nuclei [31]. Therefore, experimental results on R_{+-} for various kaonic atoms could be explained by the nature of the Λ^* resonance. More qualitative and quantitative discussions on K^- absorption in light kaonic atoms will be given in Ref. [64].

B. Nonmesonic absorption

Next we show the results of the nonmesonic absorption potential of K^- calculated with the one-meson exchange model. In the nonmesonic absorption, the Λ^* contribution appears in the $K^-pp \rightarrow (YN)^+$ and $K^-pn \rightarrow (YN)^0$ processes whereas the $K^-nn \rightarrow \Sigma^-n$ process does

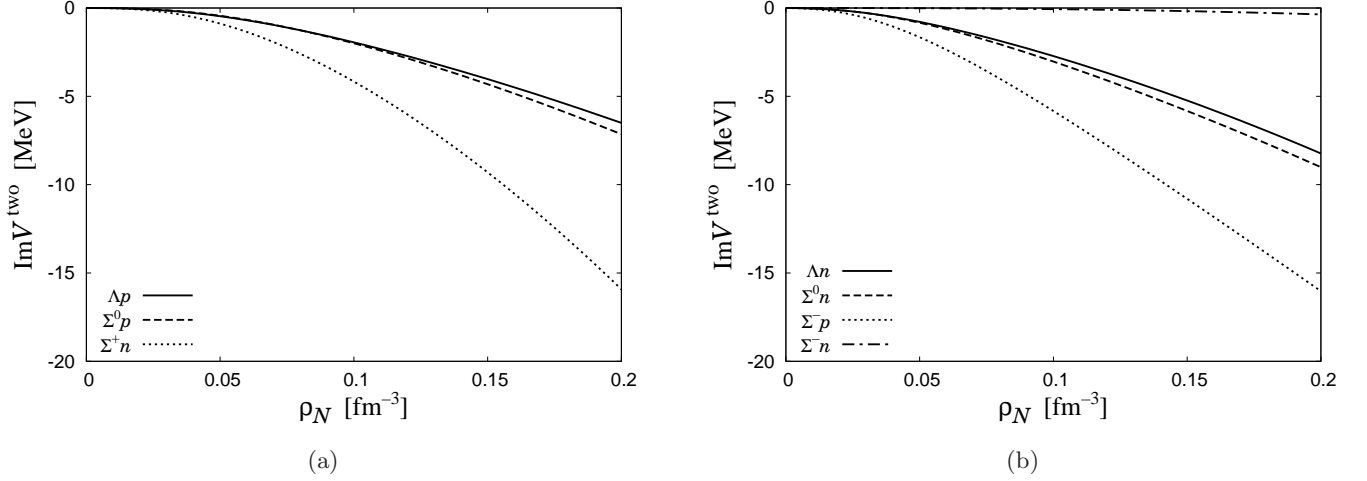


FIG. 9: Nonmesonic absorption potential ($\text{Im}V^{\text{two}}$) for K^- at rest in nuclear matter as a function of nuclear density. The contributions of the $K^-pp \rightarrow \Lambda p$, $\Sigma^0 p$, and $\Sigma^+ n$ processes (a) and of the $K^-pn \rightarrow \Lambda n$, $\Sigma^0 n$, $\Sigma^- p$ and $K^-nn \rightarrow \Sigma^- n$ processes (b).

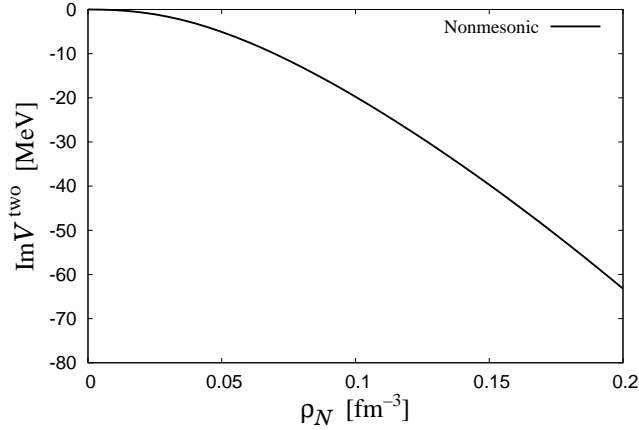


FIG. 10: Total sum of nonmesonic absorption potential ($\text{Im}V^{\text{two}}$) for K^- at rest in nuclear matter as a function of nuclear density.

not have the Λ^* contributions within the one-meson exchange picture. We also note that we expect that the nonmesonic absorption potential would be proportional to ρ_N^2 , if there is no energy nor density dependence in the KN amplitude.

The result of the nonmesonic absorption potential is shown in Fig. 9. From the figure, we find that the absorption potential has large contributions from the $K^-pp \rightarrow (YN)^+$ and $K^-pn \rightarrow (YN)^0$ processes, while the $K^-nn \rightarrow \Sigma^- n$ process gives tiny contribution. Bearing in mind that K^- absorption with a proton induces the Λ^* resonance, we see that these large contributions stem from the Λ^* resonance and the Λ^* doorway process is realized also in the nonmesonic absorption.

The total sum of the nonmesonic absorption potential is plotted in Fig. 10 as a function of nuclear den-

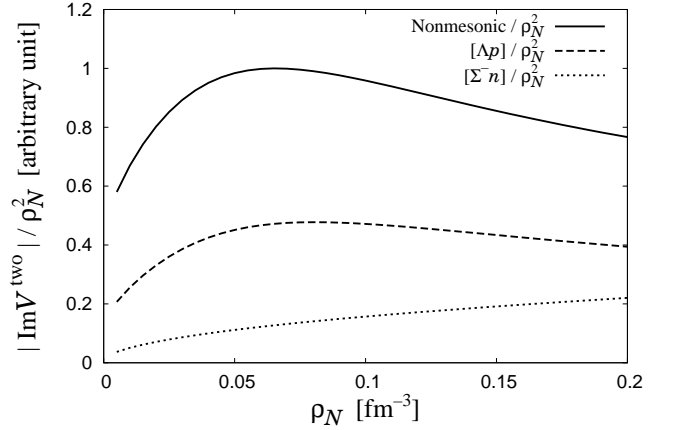


FIG. 11: Absolute absorption potentials divided by ρ_N^2 for total, Λp , and $\Sigma^- n$ contributions as functions of nuclear density in arbitrary unit. Here potentials for the Λp and $\Sigma^- n$ contributions are respectively multiplied by 5 and 50 relative to the total for comparison.

sity. The total value of the nonmesonic absorption width ($= -2\text{Im}V^{\text{two}}$) amounts to about 100 MeV at the saturation density $\rho_0 = 0.17$ fm $^{-3}$, although this value will be suppressed, as in the mesonic absorption case, when the in-medium $\bar{K}N$ scattering amplitude is employed. The total nonmesonic absorption potential has non- ρ_N^2 dependence, especially decreasing almost linearly at high densities, due to the existence of the Λ^* as doorway. Then, in a similar manner to the mesonic absorption case, we can extract the Λ^* structure by evaluating the absolute nonmesonic potentials divided by ρ_N^2 , which contains information of the squared amplitude $|\mathcal{T}|^2$ for the $K^-N \rightarrow MB$ transitions. The result is plotted in Fig. 11 for the total and the Λp and $\Sigma^- n$ nonmesonic channels.

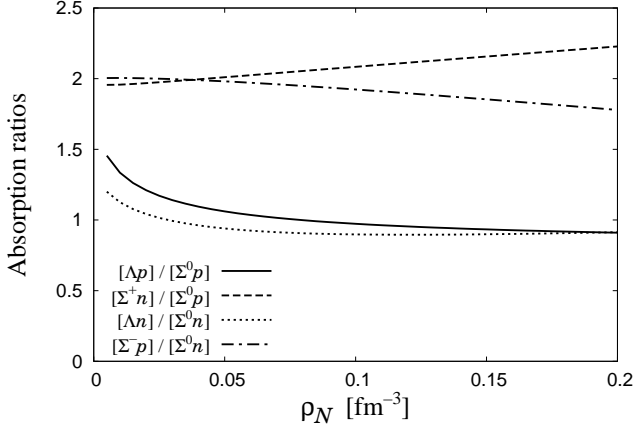


FIG. 12: Ratios of nonmesonic absorption potentials for $[\Lambda p]/[\Sigma^0 p]$, $[\Sigma^+ n]/[\Sigma^0 p]$, $[\Lambda n]/[\Sigma^0 n]$, and $[\Sigma^- p]/[\Sigma^0 n]$ as functions of nuclear density.

From the figure, while no structure appears in the $\Sigma^- n$ channel because of the absence of the Λ^* contributions, the total and Λp contributions show the peak structure around $\rho_N \approx 0.06 \text{ fm}^{-3} \approx 0.4\rho_0$, which means that the Λ^* doorway is most prosperous at these densities corresponding to the energy 1420 MeV. The peak position in Fig. 11 is consistent with the case of the mesonic absorption potential.

The dominance of the Λ^* contribution in the nonmesonic K^- absorption can also be seen in the absorption ratios $[\Lambda p]/[\Sigma^0 p]$, $[\Lambda n]/[\Sigma^0 n]$, $[\Sigma^+ n]/[\Sigma^0 p]$, and $[\Sigma^- p]/[\Sigma^0 n]$. The numerical results of our calculation for the K^- absorption are plotted as functions of nuclear density in Fig. 12. As one can see, the absorption ratios $[\Lambda p]/[\Sigma^0 p]$ and $[\Lambda n]/[\Sigma^0 n]$ in our calculation show around unity almost independently of the density. Bearing in mind that the previous study [58] on the $\Lambda^* N \rightarrow YN$ nonmesonic transition suggests the ratio of the Λ^* nonmesonic decays $[\Lambda N]/[\Sigma^0 N]$ to be around 1.2, one can see that the present results for $[\Lambda p]/[\Sigma^0 p]$ and $[\Lambda n]/[\Sigma^0 n]$ are attributed to the Λ^* dominance in K^- nonmesonic absorption. Furthermore, the K^- absorption ratio $[\Sigma^+ n]/[\Sigma^0 p]$ and $[\Sigma^- p]/[\Sigma^0 n]$ are around two in these densities in our calculation. This also suggests the Λ^* dominance, because if the initial $K^- p$ system is dominated by the $I = 0$ component these ratios should be exactly two according to the isospin symmetry. Therefore, our result of the absorption ratios shows that indeed the Λ^* doorway process dominantly contributes to the nonmesonic absorption of K^- at rest in nuclear matter.

C. Fractions of mesonic and nonmesonic absorptions

Now it is interesting to compare the magnitude of the mesonic and nonmesonic absorptions in our approach.

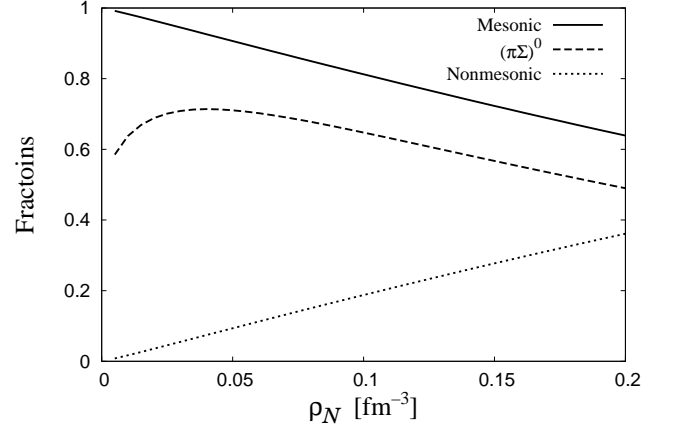


FIG. 13: Fractions of mesonic, sum of $(\pi\Sigma)^0$, and nonmesonic absorption to total absorption.

In order to see this, we show in Fig. 13 the fractions of the mesonic and nonmesonic absorptions to the total, together with the fraction of the sum of $(\pi\Sigma)^0$ states. Here we note that although the absorption potentials would be suppressed by the in-medium $\bar{K}N$ scattering amplitude, as discussed in preceding sections, the fractions of the mesonic and nonmesonic absorptions to the total would not largely change as long as the Λ^* dominance would be valid. As one can see from Fig. 13, the fraction of the mesonic (nonmesonic) absorption almost linearly goes down (up) from unity (zero) as the nuclear density increases. The reason for decrease (increase) of the fraction of the mesonic (nonmesonic) absorption is that the nonmesonic reaction can more largely contribute to the absorption at higher densities. The almost linear dependence of the fractions on density is a nontrivial result of the Λ^* properties in the Λ^* doorway process. We also note that the absorption to the $(\pi\Sigma)^0$ channels gives more than half of the total absorption process.

Beside this, we emphasize that the mesonic and nonmesonic absorption fractions are respectively about 70% and 30% at the saturation density $\rho_0 = 0.17 \text{ fm}^{-3}$ of nuclear matter. This fraction is close to the empirical value for kaonic atoms with nuclei heavier than ^4He (about 80% and 20%, respectively [24]). From Fig. 13, the nonmesonic fraction of 20% corresponds to $\rho_N = 0.1 \text{ fm}^{-3} \approx 0.6\rho_0$ in our calculation of K^- absorption at rest.

The absorption width for K^- bound in finite nuclei is obtained as the imaginary part of the eigenenergy of K^- . To obtain the eigenenergy one solves equation of motion for the K^- -nucleus system with the optical potential for K^- . Here let us estimate the nonmesonic absorption fraction for finite nuclei in an approximated way based on a perturbation theory by calculating an overlap of the absorption potential and a wave function for the bound K^- . To evaluate the wave function we need both the real and imaginary parts of the optical potential. Nevertheless, the calculation of the real part of the optical

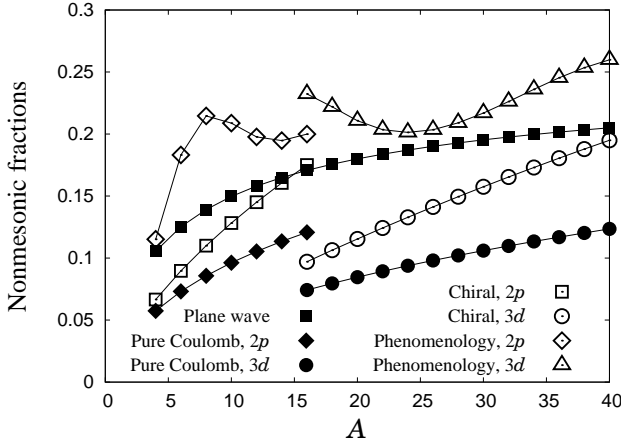


FIG. 14: Fraction of the nonmesonic absorption to the total absorption (27) for realistic nuclei with the Woods-Saxon densities. Here we consider several wave functions for kaon: $2p$ and $3d$ of the wave function in the pure Coulomb potential and in the phenomenological and chiral unitary potentials in Ref. [5], and the plane wave.

potential is out of the scope of this work, so that we take several examples for the K^- wave function. It is worth noting here that, to obtain the atomic wave function, one needs to understand the energy spectrum of the K^- nuclear states, since the wave functions of the atomic and nuclear states should be orthogonal if nuclear bound states exist, and the orthogonality condition is significant for the behavior of the wave function in the region of the nucleus size [65], where the absorption takes place. In addition, owing to the orthogonality the wave functions of the atomic states have nodes in the region of the nucleus, and this implies that K^- even in atomic states may have a large momentum inside the nucleus, as suggested in Refs. [42, 43]. It is also known that the effective density where the absorption takes place mainly is strongly dependent on the strong interaction between K^- and nucleus [66, 67].

From the nuclear density distribution, we assume the Woods-Saxon form

$$\rho_{\text{WS}}(r) \equiv \frac{\bar{\rho}}{1 + \exp[(r - R)/a]}, \quad (25)$$

where we take the nuclear radius $R = 1.18A^{1/3} - 0.48$ fm and the diffuseness $a = 0.5$ fm, which reproduce empirical density distributions of nuclei, and the normalization $\bar{\rho}$ is fixed so as to reproduce the atomic number A ,

$$A = \int d^3r \rho_{\text{WS}}(r). \quad (26)$$

Applying the local density approximation, we evaluate the absorption width as

$$\frac{\Gamma}{2} = \mathcal{N} \int d^3r |\psi(r)|^2 \text{Im}V(\rho_{\text{WS}}(r)), \quad (27)$$

where $\psi(r)$ is the K^- wave function. Here we consider several wave functions $\psi(r)$ in the $2p$ and $3d$ states, which are obtained by the pure Coulomb potential, the phenomenological potential and chiral unitary model. The latter two potentials are discussed in Ref. [5]. We also consider a plane wave with zero momentum, which could be the case of in-flight kaons with very low momentum, such 10 MeV/c.

We show in Fig. 14 the result of the nonmesonic absorption fraction to the total for nuclei of $A = 4-40$ with assumption $Z = N$. As one can see, the fractions of the nonmesonic absorption to the total absorption are marginally dependent on the wave functions. For the detail discussion, one needs to evaluate the wave functions in a more appropriate way using a realistic optical potential including the momentum dependence.

D. Absorption with finite kaon momenta and energies

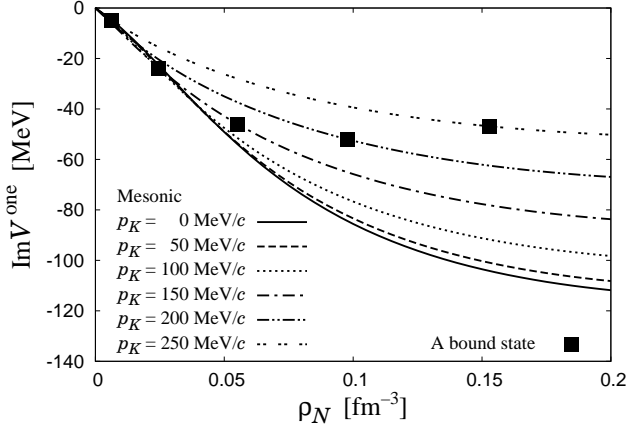
Until the previous subsections we have considered the self-energy of kaon at rest in nuclear matter with $p_{K^-}^\mu = (m_{K^-}, \mathbf{0})$. In this subsection let us take into account the finite kaon momenta $\mathbf{p}_{K^-} \neq \mathbf{0}$ and energies $E_{K^-} < m_{K^-}$. These effect will be important to investigate absorption of kaon into actual finite nuclei, because attractive strong interaction will change the kaon momentum as well as the energy from zero to finite values at the absorption point. Especially, for the atomic states, kaons in the center of the nucleus may have large momenta to compensate a large strong attraction by the kaon kinetic energy for small atomic binding energy as suggested in Ref. [42, 43].

One important influence of the finite kaon momenta and energies is the downward shift of the K^-N two-body energy W (11) due to the off-shellness of kaon. Actually for the kaon energy-momentum $p_{K^-}^\mu = (E_{K^-}, \mathbf{p}_{K^-})$ the two-body energy W becomes, after averaging the angular dependence,

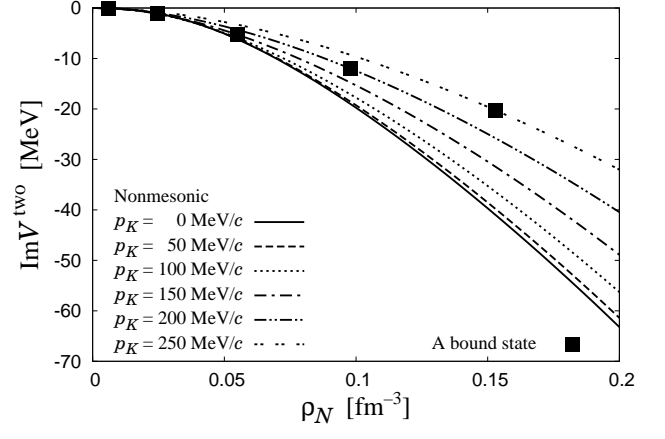
$$W = \sqrt{(E_1 + E_{K^-})^2 - p_1^2 - p_{K^-}^2}, \quad (28)$$

which is obviously smaller than W with $E_{K^-} = m_{K^-}$ and $\mathbf{p}_{K^-} = \mathbf{0}$. This fact indicates that the nuclear density which hits Λ^* will become lower according to the values of $p_{K^-}^2$ and E_{K^-} . Here we will see how this two-body energy shift affects the absorption scenarios with finite kaon momenta and energies.

Firstly we consider the finite kaon momenta with $p_{K^-}^\mu = (m_{K^-}, \mathbf{p}_{K^-})$. Here we take the approximation that we average the angular dependence appearing in the K^-NN three-body energy E_{tot} in the nonmesonic absorption as well as the K^-N two-body energy W so that one drops the angular dependence of $\mathbf{p}_{K^-} \cdot \mathbf{p}_1$ and $\mathbf{p}_{K^-} \cdot \mathbf{p}_2$ with initial nucleon momenta \mathbf{p}_1 and \mathbf{p}_2 . The mesonic and nonmesonic absorption potentials with finite kaon momenta are shown in Fig. 15 from $p_{K^-} = 0$ MeV/c, which is the same case as the previous subsections, to

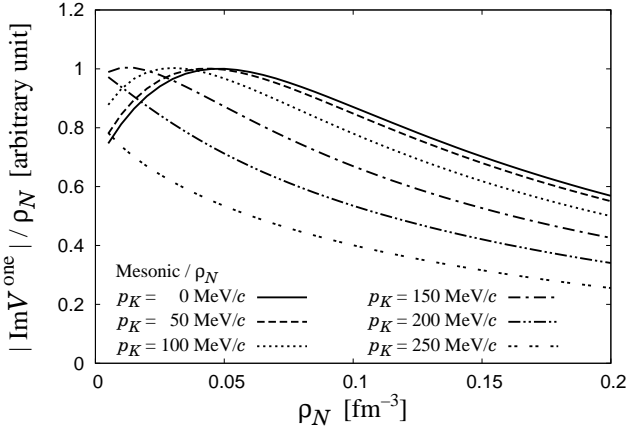


(a)

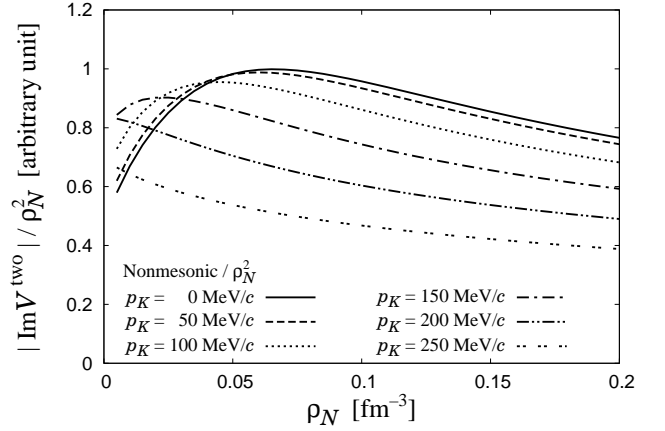


(b)

FIG. 15: Mesonic (a) and nonmesonic (b) absorption potentials with finite kaon momenta p_{K-} . A bound state case given in Eqs. (29) and (30) is indicated by the filled squares.



(a)



(b)

FIG. 16: Absolute absorption potentials with finite kaon momenta p_{K-} divided by ρ_N for mesonic case (a) and divided by ρ_N^2 for nonmesonic case (b) in arbitrary unit.

$p_{K-} = 250$ MeV/c. As one can see, the absorption potentials become weaker as the kaon momentum increases in both mesonic and nonmesonic cases. While with the small kaon momenta $p_{K-} \lesssim 100$ MeV/c the absorption potentials are suppressed only slightly, the potentials with $p_{K-} \gtrsim 200$ MeV/c become about half of the potential with kaon at rest at the nuclear saturation density.

For the bound state, since it is an eigenstate, the momentum and position of the kaon are correlated. If one takes the local density approximation, which connects position and density, the density and momentum can be also correlated. Therefore, each bound state may have one line for the absorption strength against the density. As an example, we put squares in Fig. 15 for a bound kaon atomic state calculated with a density-momentum

relation,

$$\frac{p_{K-}(\rho_N)^2}{2m_K} + \text{Re}V(\rho_N) = -(\text{atomic binding energy}) \approx 0. \quad (29)$$

where we take a potential proportional to the nuclear density with a typical potential strength from the chiral unitary approach,

$$\text{Re}V(\rho_N) = -70 \text{ MeV} \times \frac{\rho_N}{\rho_0}. \quad (30)$$

The squares show that the growth of the absorption potentials become decrease as the nuclear density gets large compared to the case of kaon at rest due to the increase of p_{K-} as a function of the nuclear density. The squares will move upward (downward) in the figure as the potential strength becomes strong (weak).

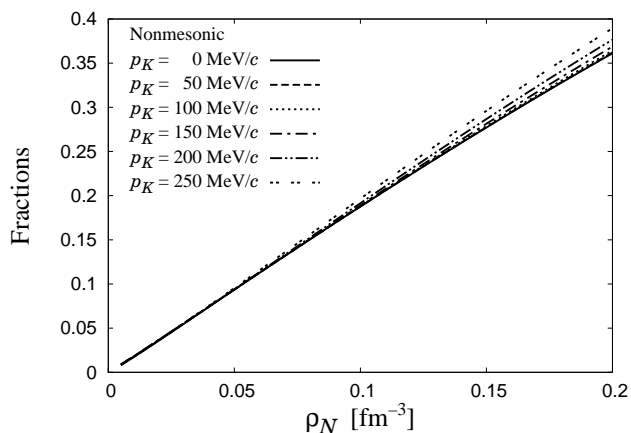


FIG. 17: Fraction of the nonmesonic absorption to the total absorption with finite kaon momenta p_{K^-} .

The suppression of the absorption potential is caused by the two reasons. One is, as we have already mentioned, the downward shift of the two-body energy W due to the finite p_{K^-} makes the nuclear density which hits the Λ^* resonance lower, and hence the Λ^* doorway becomes weak compared to the case of kaon at rest at the saturation density. Indeed, we can estimate the density at which the Λ^* contribution is large by calculating $|\text{Im}V^{\text{one}}|/\rho_N$ and $|\text{Im}V^{\text{two}}|/\rho_N^2$, and the results with finite kaon momenta is plotted in Fig. 16. From the figure, one can see the peak position shifts downward density as the kaon momentum increases, which is consistent with the expectation from behavior of W , and the peak disappears at $p_{K^-} \sim 200$ MeV/c because in such kaon momenta the two-body energy W is smaller than the Λ^* peak position even in the low density limit, $\rho_N \rightarrow 0$. The other reason for the suppression of the absorption potential is that the downward shift of W makes the phase space for the on-shell πY mesonic channels and YN nonmesonic channels small and hence suppresses the reaction rate for the absorption, $\gamma_{\pi Y, YN}$. We have checked that these two factors suppresses the absorption potential with similar strength. We note that the phase-space suppression is especially crucial to the mesonic absorption because the W is closer to the πY threshold in the mesonic case than the E_{tot} to the YN threshold in the nonmesonic case.

The fraction of nonmesonic absorption to the total absorption with finite kaon momenta is plotted in Fig. 17. The figure indicates that, although the absolute absorption potentials are suppressed due to the finite kaon momenta both in the mesonic and nonmesonic cases, the fraction only slightly changes because of the cancellation of the suppressions. This means that the results for the nonmesonic fraction obtained in the previous subsection is not so sensitive to the kaon momentum.

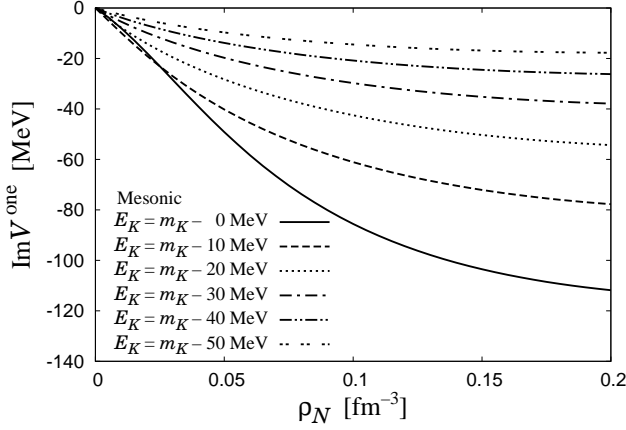
Next let us take into account the kaon energy. Here we assume the kaon is at rest with energy $E_{K^-} < m_{\bar{K}}$,

$p_{K^-}^\mu = (E_{K^-}, \mathbf{0})$. The mesonic and nonmesonic absorption potentials with the finite kaon energies are plotted in Fig. 18 up to $m_{\bar{K}} - 50$ MeV. From the figure, one can see the suppression for the absorption potentials in a similar manner to the finite kaon momentum case. For the finite kaon energy, the absorption potentials are largely suppressed even at $E_{K^-} = m_{\bar{K}} - 10$ MeV, which reflects that the energy shift due to that energy is large enough to suppress the Λ^* doorway contribution and the phase space for the decay channel. In both mesonic and nonmesonic cases, the absorption potentials at the saturation density becomes half for the kaon energy $E_{K^-} \sim m_{\bar{K}} - 20$ MeV compared to the potential for kaon with $E_{K^-} = m_{\bar{K}}$. The fraction of nonmesonic absorption to the total absorption with finite kaon energies is plotted in Fig. 19. The nonmesonic fraction increases as the energy decreases, and at the saturation density the fraction becomes ~ 0.4 with $E_{K^-} = m_{\bar{K}} - 50$ MeV while it is ~ 0.3 for kaon with $E_{K^-} = m_{\bar{K}}$.

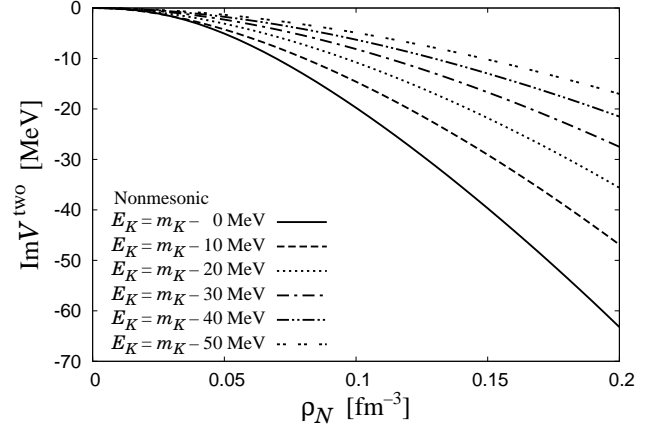
Finally we summarize our results for the K^- absorption potential with the s -wave $\bar{K}N \rightarrow MB$ transition amplitude. We have seen that K^- absorption at rest is dominated by the Λ^* doorway process, where the transitions of the initial state K^-N to MB take place mainly through the Λ^* resonance. From the behavior of the absorption potential the Λ^* contributes mostly at the nuclear density $\rho_N \approx 0.05\text{--}0.06$ fm $^{-3}$. We have found that increase of the ratio $[\pi^-\Sigma^+]/[\pi^+\Sigma^-]$ in experiments of heavier kaonic atoms can be explained as the interference with the nonresonant $I = 1$ background with respect to the Λ^* contributions in the $\bar{K}N$ subthreshold region. Due to the dominance of the Λ^* doorway process, the nonmesonic absorption ratios $[\Lambda p]/[\Sigma^0 p]$ and $[\Lambda n]/[\Sigma^0 n]$ are about unity while $[\Sigma^+ n]/[\Sigma^0 p]$ and $[\Sigma^- p]/[\Sigma^0 n]$ are about two. In addition, our approach gives that the mesonic and nonmesonic absorption fractions are respectively about 70% and 30% at the saturation density. Estimating the surface effect for finite nuclei with some examples of the K^- wave function, we have found that the fraction of the nonmesonic absorption will be about 10–20%. The details are dependent on the atomic wave function, and thus more realistic evaluation is necessary with real part of the optical potential. Taking into account the kaon momenta and the kaon energies, the absorption potentials become weaker due to the downward shift of the K^-N two-body energy. However, even in such a case the fraction of the nonmesonic absorption does not drastically change because of the cancellation of the suppressions of potentials.

IV. $\Sigma(1385)$ CONTRIBUTIONS

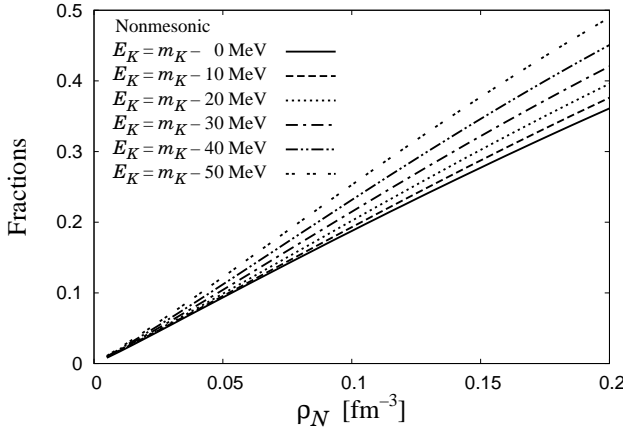
Next we examine the $\Sigma(1385)$ (Σ^*) contribution to K^- absorption. The hyperon resonance Σ^* exists below the $\bar{K}N$ threshold and couples to $\bar{K}N$ and πY channels in p wave. Since the scattering amplitude with p -wave coupling is proportional to the momentum transfer, we ex-



(a)



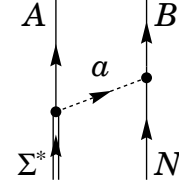
(b)

FIG. 18: Mesonic (a) and nonmesonic (b) absorption potentials with kaon energy $E_K < m_{\bar{K}}$.FIG. 19: Fraction of the nonmesonic absorption to the total absorption with kaon energy $E_K < m_{\bar{K}}$.

pect that the Σ^* contribution to the K^- absorption with small kaon momenta is small compared to the Λ^* contribution, which couples to $\bar{K}N$ and $\pi\Sigma$ channels in s wave. Here we also discuss the Σ^* nonmesonic decay in nuclear matter in the similar manner to the Λ^* resonance developed in Ref. [58]. Because we are interested in the K^- absorption in nuclear matter, we take into account Σ^{*0} and Σ^{*-} contributions, while Σ^{*+} is not considered in this study since it is not directly produced in the K^-N initial state. Throughout this study we neglect in-medium modifications on Σ^* .

A. $\Sigma(1385)$ -induced nonmesonic decay

Before going to the K^- absorption, we discuss the nonmesonic decay process of Σ^* in nuclear matter by considering the $\Sigma^*N \rightarrow YN$ transition in the nuclear medium. This enables us to investigate the nonmesonic

FIG. 20: Feynman diagram for the $\Sigma^*N \rightarrow YN$ process. The propagating particles a , A , and B are listed in Table III.

decay pattern for the Σ^* dominance, and is a supplemental study with respect to the Λ^* -induced nonmesonic decay discussed in Ref. [58]. For this purpose, we calculate the $\Sigma^*N \rightarrow YN$ process ($\Sigma^{*0}p \rightarrow \Lambda p$, $\Sigma^{*0}p \rightarrow \Sigma^+n$, $\Sigma^{*0}n \rightarrow \Lambda n$, $\Sigma^{*0}n \rightarrow \Sigma^0n$, and $\Sigma^{*-}p \rightarrow \Lambda n$, $\Sigma^{*-}p \rightarrow \Sigma^0n$, and $\Sigma^{*-}p \rightarrow \Sigma^-n$) in uniform nuclear matter with a one-meson exchange approach, as done in Ref. [58]. Here we note that we have two cases of initial states, $\Sigma^{*0}n$ and $\Sigma^{*-}p$, for the $(YN)^0$ final states.

In this study we use one-meson exchange model diagrammatically shown in Fig. 20 with propagating particles listed in Table III. Along with the Λ^* -induced nonmesonic decay discussed in Ref. [58], we define the nonmesonic decay width of Σ^* in nuclear matter through the $\Sigma^*N \rightarrow YN$ process, $\Gamma_{\Sigma^*N \rightarrow YN}$, as,

$$\Gamma_{\Sigma^*N \rightarrow YN} = \int_0^{k_F} \frac{dp_1 p_1^2}{\pi^2} \sum_{\lambda} \sum_{\lambda'} \gamma_{\Sigma^*N \rightarrow YN}, \quad (31)$$

$$\gamma_{\Sigma^*N \rightarrow YN} \equiv \frac{p_{\text{cm}}'' M_Y M_N}{4\pi^2 E_{\text{tot}}} \int d\Omega_N |\mathcal{B}_{YN}|^2, \quad (32)$$

where \mathcal{B}_{YN} is the scattering amplitude for the $\Sigma^*N \rightarrow YN$ process written as,

$$\mathcal{B}_{YN} = \sum_i \xi_i \mathcal{B}_i (\Sigma_i^* N_i \xrightarrow{a_i} A_i B_i) \quad (33)$$

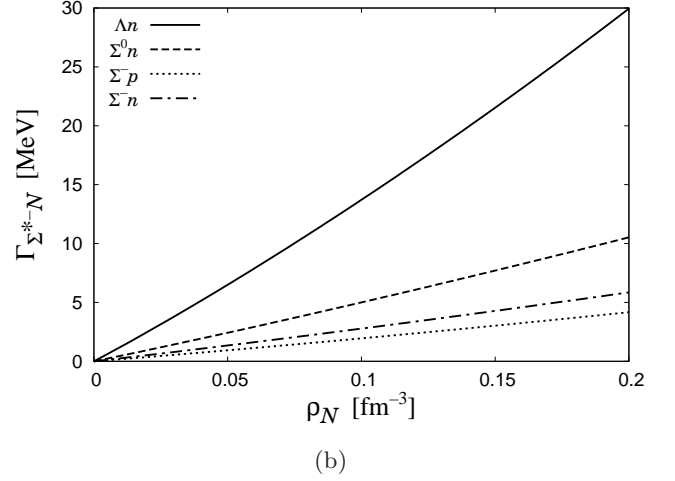
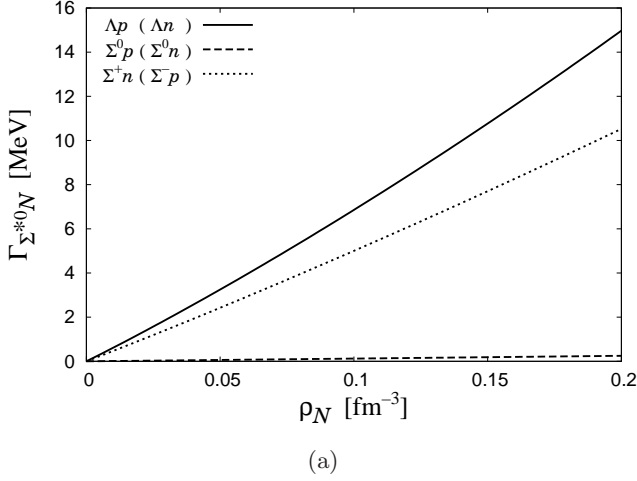


FIG. 21: The Σ^* -induced nonmesonic decay width as a function of nuclear density. (a) and (b) shows the Σ^{*0} and Σ^{*-} contributions, respectively.

TABLE III: Possible channels for Eq. (33). Here Σ^* and N are the hyperon resonance and nucleon in the initial state, while A and B are the baryons in the final state. a denotes the exchange meson. ξ is the relative sign of the amplitude coming from the exchange of the final state baryons. C is the Clebsch-Gordan coefficients for the $aA\Sigma^*$ coupling, and α and β are the Clebsch-Gordan coefficients for the BBM coupling.

Σ^*	N	a	A	B	ξ	C_{aA}	α	β
Σ^{*0}	p	K^-	p	Λ	$+$	$-\sqrt{1/12}$	$-2/\sqrt{3}$	$1/\sqrt{3}$
		π^0	Λ	p	$-$	$1/2$	1	0
Σ^{*0}	p	K^-	p	Σ^0	$+$	$-\sqrt{1/12}$	0	1
		η	Σ^0	p	$-$	$-1/2$	$1/\sqrt{3}$	$-2/\sqrt{3}$
Σ^{*0}	p	\bar{K}^0	n	Σ^+	$+$	$\sqrt{1/12}$	0	$\sqrt{2}$
		π^-	Σ^+	n	$-$	$\sqrt{1/12}$	$\sqrt{2}$	0
Σ^{*0}	n	\bar{K}^0	n	Λ	$+$	$\sqrt{1/12}$	$-2/\sqrt{3}$	$1/\sqrt{3}$
		π^0	Λ	n	$-$	$1/2$	-1	0
Σ^{*0}	n	\bar{K}^0	n	Σ^0	$+$	$\sqrt{1/12}$	0	-1
		η	Σ^0	n	$-$	$-1/2$	$1/\sqrt{3}$	$-2/\sqrt{3}$
Σ^{*0}	n	K^-	p	Σ^-	$+$	$-\sqrt{1/12}$	0	$\sqrt{2}$
		π^+	Σ^-	p	$-$	$-\sqrt{1/12}$	$\sqrt{2}$	0
Σ^{*-}	p	K^-	n	Λ	$+$	$-\sqrt{1/6}$	$-2/\sqrt{3}$	$1/\sqrt{3}$
		π^-	Λ	n	$-$	$1/2$	$\sqrt{2}$	0
Σ^{*-}	p	K^-	n	Σ^0	$+$	$-\sqrt{1/6}$	0	1
		π^-	Σ^0	n	$-$	$-\sqrt{1/12}$	$\sqrt{2}$	0
Σ^{*-}	p	π^0	Σ^-	p	$-$	$\sqrt{1/12}$	1	0
		η	Σ^-	p	$-$	$-1/2$	$1/\sqrt{3}$	$-2/\sqrt{3}$
Σ^{*-}	n	K^-	n	Σ^-	$+$	$-\sqrt{1/6}$	0	$\sqrt{2}$
		π^0	Σ^-	n	$-$	$\sqrt{1/12}$	-1	0
		η	Σ^-	n	$-$	$-1/2$	$1/\sqrt{3}$	$-2/\sqrt{3}$

for channel i with an amplitude for $\Sigma^*N \xrightarrow{a} AB$ process,

$$\mathcal{B}(\Sigma^*N \xrightarrow{a} AB) = iD_{aA} \times \tilde{\Pi}_a^{(p)}(q_a^2; \mathbf{q}_a, \mathbf{S}_1, \boldsymbol{\sigma}_2) \times \tilde{V}_{aNB}. \quad (34)$$

Here the symbol ξ denotes relative sign of the amplitude

coming from the exchange of the final-state baryons, a denotes the propagating meson, and D_{aA} is the $aA\Sigma^*$ coupling constant, which we evaluate by first using the SU(6) quark model to relate the πNN coupling to the $\pi N\Delta$ one and then using the flavor SU(3) symmetry to relate the $\pi N\Delta$ coupling to the $\pi Y\Sigma^*$, $\eta Y\Sigma^*$, and $\bar{K}N\Sigma^*$ ones, as done in Ref. [68], and as a result we obtain,

$$D_{aA} = C_{aA} \frac{12}{5} \frac{D+F}{2f}, \quad (35)$$

with the SU(3) coefficient C_{aA} listed in Table III and parameters $D+F=1.26$ and $f=f_\pi=93.0$ MeV. The propagator with p -wave short-range correlation $\tilde{\Pi}_a^{(p)}$ is written as [62],

$$\begin{aligned} \tilde{\Pi}_a^{(p)}(q^2; \mathbf{q}, \mathbf{S}, \boldsymbol{\sigma}) \\ = (\mathbf{q} \cdot \mathbf{S})(\mathbf{q} \cdot \boldsymbol{\sigma}) \tilde{\Pi}_a(q^2) - \mathbf{S} \cdot \boldsymbol{\sigma} \frac{q_C^2}{3} \left(\frac{\Lambda^2}{\Lambda^2 - \tilde{q}^2} \right)^2 \frac{1}{\tilde{q}^2 - m_a^2}. \end{aligned} \quad (36)$$

We use here the same parameters $\Lambda=1.0$ GeV and $q_C=780$ MeV as for the s -wave short-range correlations. For the MBB coupling \tilde{V} we use the same one as in the previous section,

$$\tilde{V}_{aNB} = \alpha_{aNB} \frac{D+F}{2f} + \beta_{aNB} \frac{D-F}{2f}. \quad (37)$$

The vector \mathbf{S} is the spin transition operator from spin $3/2$ to $1/2$ having a relation,

$$S^i S^{j\dagger} = \frac{2}{3} \delta^{ij} - \frac{i}{3} \epsilon_{ijk} \sigma^k. \quad (38)$$

The subscript 1 (2) for the operator \mathbf{S} ($\boldsymbol{\sigma}$) in Eq. (34) means that the operator is sandwiched by the spinors for Σ^* and A (N and B). The Σ^* mass is fixed as 1385 MeV.

The results of the nonmesonic decay width of Σ^{*0} and Σ^{*-} in nuclear matter is shown in Fig. 21. The linear dependence of the decay widths is caused by insensitivity of the elementary transition rate $\gamma_{\Sigma^*N \rightarrow YN}$ to the Fermi motion of the initial nucleon. For the Σ^* -induced nonmesonic decays, there are several relations due to the flavor SU(3) symmetry in the coupling constants. In the Σ^{*0} case we obtain the same result for proton and neutron in initial state because of the same coupling strengths in the scattering amplitudes, hence we plot them in one figure [Fig. 21(a)]. We also find that $\Gamma_{\Sigma^{*0}N \rightarrow \Lambda N} / \Gamma_{\Sigma^{*-}p \rightarrow \Lambda n} = 1/2$ and $\Gamma_{\Sigma^{*0}N \rightarrow \Sigma^+ N} / \Gamma_{\Sigma^{*-}p \rightarrow \Sigma^0 n} = 1$.

One interesting finding is that at all densities the Σ^* -induced nonmesonic decay ratio $\Gamma_{\Lambda N} / \Gamma_{\Sigma^0 N}$ is much larger than the Λ^* -induced one ≈ 1.2 [58]. Especially in the Σ^{*0} -induced case, we have very small branching ratio to the $\Sigma^0 N$ final state. This is caused by the small couplings \tilde{V} at both $\bar{K}N\Sigma^0$ and ηNN vertices in the $\Sigma^{*0}N \rightarrow \Sigma^0 N$ transition, hence the Σ^{*0} scarcely exchanges one Nambu-Goldstone boson for the Σ^0 final states. Also it should be noted that there is no relation between the $\Sigma^0 p$ ($\Sigma^0 n$) and $\Sigma^+ n$ ($\Sigma^- p$) branching ratios, which should be 1/2 if the $I = 0$ hyperon resonance appears in the initial state. These points will be important in the discussion of the Λ^*/Σ^* contribution rate in the realistic kaon absorption experiments.

At the saturation density $\rho_0 = 0.17 \text{ fm}^{-3}$, the total nonmesonic decay width is 43 MeV (42 MeV) for Σ^{*0} (Σ^{*-}), in which $\Gamma_{\Lambda p} + \Gamma_{\Lambda n} = 25 \text{ MeV}$, $\Gamma_{\Sigma^0 p} + \Gamma_{\Sigma^0 n} = 0.4 \text{ MeV}$, and $\Gamma_{\Sigma^+ n} + \Gamma_{\Sigma^- p} = 17 \text{ MeV}$ ($\Gamma_{\Lambda n} = 25 \text{ MeV}$, $\Gamma_{\Sigma^0 n} = 9 \text{ MeV}$, $\Gamma_{\Sigma^- p} = 3 \text{ MeV}$, and $\Gamma_{\Sigma^- n} = 5 \text{ MeV}$). They are similar to the mesonic Σ^* decay width in vacuum $\approx 37 \text{ MeV}$.

B. $\Sigma(1385)$ contribution to antikaon absorption

Let us evaluate how the Σ^* contributes the K^- absorption in nuclear matter. For this purpose, we add coherently the Σ^* contribution in the simple Breit-Wigner form as,

$$\mathcal{T}_{\pi Y}^{(\Sigma^*)}(W) = (\mathbf{p}_\pi \cdot \mathbf{S}_1) \frac{D_{\pi Y} D_{K^- N_1}}{W - M_{\Sigma^*} + i\Gamma_{\Sigma^*}/2} (\mathbf{p}_{K^-} \cdot \mathbf{S}_1^\dagger), \quad (39)$$

for mesonic absorption and,

$$\begin{aligned} \mathcal{A}^{(\Sigma^*)}(K^- N_1 N_2 \xrightarrow{a} AB) \\ = \frac{\tilde{V}_{aN_2 B} D_{aA} D_{K^- N_1}}{W - M_{\Sigma^*} + i\Gamma_{\Sigma^*}/2} \tilde{\Pi}_a^{(p)}(q_a^2; \mathbf{q}, \mathbf{S}_1, \boldsymbol{\sigma}_2) (\mathbf{p}_{K^-} \cdot \mathbf{S}_1^\dagger), \end{aligned} \quad (40)$$

for nonmesonic absorption. Here $M_{\Sigma^*} = 1385 \text{ MeV}$ and $\Gamma_{\Sigma^*} = 37 \text{ MeV}$ are mass and decay width of Σ^* , respectively, and the subscript 1 in the $\mathbf{S}^{(\dagger)}$ denotes to be sandwiched by the spinors for N_1 and A .

The results for kaon energy-momentum $p_{K^-}^\mu = (m_{\bar{K}}, \mathbf{p}_{K^-})$ with momenta $p_{K^-} \equiv \mathbf{p}_{K^-} = 0 \text{ MeV}/c$ and

100 MeV/c are shown in Fig. 22. As we can see, the Σ^* contributions are constructively added to the absorption potential. However, the values of the contribution to the potential are quite small compared with the Λ^* one for the kaon at rest, $p_{K^-} = 0 \text{ MeV}/c$, and even for $p_{K^-} = 100 \text{ MeV}/c$ the shift of the absorption potential at the nuclear saturation density is less than 10 MeV both in mesonic and nonmesonic cases. This feature has been seen also in the \bar{K} -nucleus bound systems [69, 70] and the analysis of the kaonic atoms data [43]. This is because Σ^* sits energy farther below the $\bar{K}N$ threshold than Λ^* and Σ^* exists in p wave of K^-N system and hence requires high momentum transfer, which is not adequately achieved with slow K^- and Fermi momentum of N . Thus, we can neglect the Σ^* contribution to the absorption of slow K^- .

V. SUMMARY

In this paper we have theoretically investigated the branching ratios of mesonic and nonmesonic K^- absorption in nuclear matter in order to understand the mechanism of K^- absorption in experiments by systematic evaluation of the decay patterns of \bar{K} -nucleus systems from the low-energy $\bar{K}N$ interaction. For the K^- absorption, we have paid attention to two hyperon resonances, Λ^* and Σ^* , which are both below and close to the $\bar{K}N$ threshold and thus will play important roles in the absorption process. The mesonic and nonmesonic absorption is evaluated from the K^- self-energy with one- and two-nucleon interactions, respectively, which are the most probable contributions at moderate nuclear densities.

As a result, within s -wave $\bar{K}N$ scatterings determined by the chiral unitary approach, which dynamically generates Λ^* , we have seen that both the mesonic and nonmesonic K^- absorption potentials at rest are dominated by the Λ^* doorway process in the $K^-p \rightarrow MB$ scattering. The density dependence of the K^- absorption potential shows non- ρ_N^1 (non- ρ_N^2) dependence due to the existence of the Λ^* resonance in mesonic (nonmesonic) absorption process. We have found that the interference between Λ^* and the nonresonant $I = 1$ background modifies transition strengths of K^-p to $\pi^+\Sigma^-$, $\pi^-\Sigma^+$, and $\pi^0\Sigma^0$ channels below the threshold and this modification can explain the ratios $[\pi^-\Sigma^+]/[\pi^+\Sigma^-]$ (R_{+-}) of the branching ratios observed in several kaonic atoms in experiments. Due to the Λ^* dominance doorway process, the nonmesonic absorption ratios $[\Lambda p]/[\Sigma^0 p]$ and $[\Lambda n]/[\Sigma^0 n]$ are about unity while $[\Sigma^+ n]/[\Sigma^0 p]$ and $[\Sigma^- p]/[\Sigma^0 n]$ are about two. Our approach gives that the mesonic and nonmesonic absorption fractions are respectively about 70% and 30% at the saturation density, and with some K^- atomic wave functions and the Woods-Saxon density distribution we obtain the fraction ~ 10 –20% for the nonmesonic absorption. Taking into account the kaon momenta and the energies, the absorption potentials become

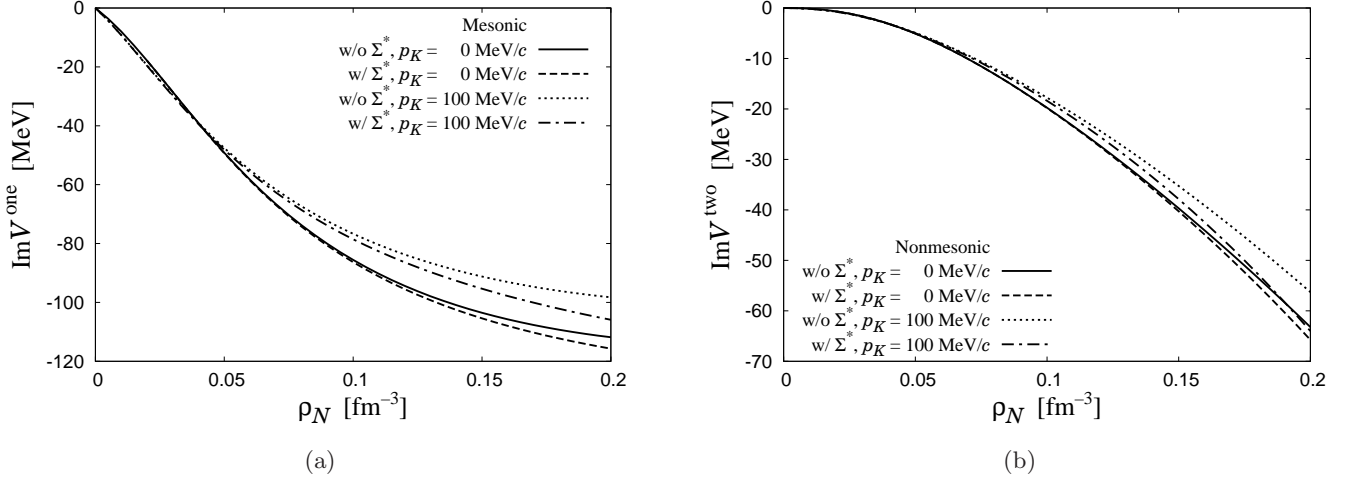


FIG. 22: Total mesonic and nonmesonic absorption potentials [$\text{Im}V^{\text{one}}$ (a) and $\text{Im}V^{\text{two}}$ (b), respectively] for K^- in nuclear matter as functions of nuclear density. Here we plot without and with Σ^* contributions in the $K^-N \rightarrow MB$ amplitude, and we take the kaon momentum $p_{K^-} = 0$ MeV/c and 100 MeV/c.

weaker due to the downward shift of the initial K^-N two-body energy, but this does not drastically change the nonmesonic fraction.

We note that the density dependence of the decay pattern will be realized by using nuclei with different atomic numbers as targets of stopped K^- reaction. Especially the light nuclei such as the deuteron, ^3He , and ^4He will be suitable for this purpose, since they serve as environment of various nuclear densities inside nuclei due to the large varieties of the binding energies per one nucleon.

From the discussions on the Σ^* contribution we have observed different branching ratios and the larger total width in the Σ^* -induced nonmesonic decay, where one Σ^* exists in nuclear medium in its initial state, compared with the Λ^* -induced one discussed in the previous study [58]. This fact will be important in the discussion on Λ^*/Σ^* contribution rate in the realistic \bar{K} absorption experiments. In the slow K^- absorption up to the momentum 100 MeV/c, however, Σ^* has very small contributions to the absorption process, because Σ^* exists in

p wave of the K^-N system and requires high momentum transfer, which is not adequately achieved with slow K^- and the Fermi momentum of N . As a consequence, Λ^* in the s -wave K^-p system gives dominant contributions to slow K^- absorption.

Acknowledgments

We acknowledge A. Ohnishi and K. Yazaki for useful discussions. This work is partly supported by the Grand-in-Aid for Scientific Research from MEXT and JSPS (Nos. 22740161, 22-3389, and 24105706), and the Grant-in-Aid for the Global COE Program “The Next Generation of Physics, Spun from Universality and Emergence” from MEXT of Japan. One of the authors, T.S. acknowledges the support by the Grand-in-Aid from JSPS. This work is part of the Yukawa International Program for Quark-Hadron Sciences (YIPQS).

-
- [1] R. H. Dalitz, T. C. Wong and G. Rajasekaran, Phys. Rev. **153**, 1617 (1967).
 - [2] T. Hyodo and D. Jido, Prog. Part. Nucl. Phys. **67**, 55 (2012).
 - [3] T. Kishimoto, Phys. Rev. Lett. **83**, 4701 (1999).
 - [4] Y. Akaishi and T. Yamazaki, Phys. Rev. C **65**, 044005 (2002).
 - [5] J. Yamagata, H. Nagahiro and S. Hirenzaki, Phys. Rev. C **74**, 014604 (2006).
 - [6] N. V. Shevchenko, A. Gal and J. Mares, Phys. Rev. Lett. **98**, 082301 (2007).
 - [7] Y. Ikeda and T. Sato, Phys. Rev. C **76**, 035203 (2007).
 - [8] A. Dote, T. Hyodo and W. Weise, Nucl. Phys. A **804**, 197 (2008).
 - [9] S. Wycech and A. M. Green, Phys. Rev. C **79**, 014001 (2009).
 - [10] M. Bayar, J. Yamagata-Sekihara and E. Oset, Phys. Rev. C **84**, 015209 (2011).
 - [11] D. Jido and Y. Kanada-En'yo, Phys. Rev. C **78**, 035203 (2008).
 - [12] A. Martinez Torres, K. P. Khemchandani and E. Oset, Phys. Rev. C **79**, 065207 (2009).
 - [13] A. Martinez Torres and D. Jido, Phys. Rev. C **82**, 038202 (2010).
 - [14] J. -J. Xie, A. Martinez Torres and E. Oset, Phys. Rev. C **83**, 065207 (2011).
 - [15] Y. Kanada-En'yo and D. Jido, Phys. Rev. C **78**, 025212 (2008).

- [16] V. Koch, Phys. Lett. B **337**, 7 (1994).
- [17] T. Waas, N. Kaiser and W. Weise, Phys. Lett. B **365**, 12 (1996).
- [18] T. Waas, N. Kaiser and W. Weise, Phys. Lett. B **379**, 34 (1996).
- [19] T. Waas and W. Weise, Nucl. Phys. A **625**, 287 (1997).
- [20] M. Lutz, Phys. Lett. B **426**, 12 (1998).
- [21] A. Ramos and E. Oset, Nucl. Phys. A **671**, 481 (2000).
- [22] D. B. Kaplan and A. E. Nelson, Phys. Lett. B **175**, 57 (1986).
- [23] C. J. Batty, E. Friedman and A. Gal, Phys. Rept. **287**, 385 (1997).
- [24] E. Friedman and A. Gal, Phys. Rept. **452**, 89 (2007).
- [25] D. N. Tovee, D. H. Davis, J. Simonovic, G. Bohm, J. Klabuhn, F. Wysotzki, M. Csejthey-Barth and J. H. Wickens *et al.*, Nucl. Phys. B **33**, 493 (1971).
- [26] R. J. Nowak, J. Armstrong, D. H. Davis, D. J. Miller, D. N. Tovee, D. Bertrand, M. Goossens and G. Vanhomwegen *et al.*, Nucl. Phys. B **139**, 61 (1978).
- [27] V. R. Veirs and R. A. Burnstein, Phys. Rev. D **1**, 1883 (1970).
- [28] P. A. Katz, K. Bunnell, M. Derrick, T. Fields, L. G. Hyman and G. Keyes, Phys. Rev. D **1**, 1267 (1970).
- [29] C. Vander Velde-Wilquet, J. Sacton, J. H. Wickens, D. N. Tovee and D. H. Davis, Nuovo Cim. A **39**, 538 (1977).
- [30] T. Onaga, H. Narumi and T. Kohmura, Prog. Theor. Phys. **82**, 222 (1989).
- [31] M. Agnello *et al.* [FINUDA Collaboration], Phys. Lett. B **704**, 474 (2011).
- [32] L. R. Staronski and S. Wycech, J. Phys. G **13**, 1361 (1987).
- [33] A. Ohnishi, Y. Nara and V. Koch, Phys. Rev. C **56**, 2767 (1997).
- [34] M. Iwasaki, R. S. Hayano, T. M. Ito, S. N. Nakamura, T. P. Terada, D. R. Gill, L. Lee and A. Olin *et al.*, Phys. Rev. Lett. **78**, 3067 (1997).
- [35] T. M. Ito, R. S. Hayano, S. N. Nakamura, T. P. Terada, M. Iwasaki, D. R. Gill, L. Lee and A. Olin *et al.*, Phys. Rev. C **58**, 2366 (1998).
- [36] G. Beer *et al.* [DEAR Collaboration], Phys. Rev. Lett. **94**, 212302 (2005).
- [37] M. Bazzi, *et al.* [SIDDHARTA Collaboration], Phys. Lett. B **704**, 113 (2011).
- [38] M. Bazzi, *et al.* [SIDDHARTA Collaboration], Nucl. Phys. A **881**, 88 (2012).
- [39] Y. Ikeda, T. Hyodo and W. Weise, Phys. Lett. B **706**, 63 (2011).
- [40] Y. Ikeda, T. Hyodo and W. Weise, Nucl. Phys. A **881**, 98 (2012).
- [41] M. Mai and U. -G. Meissner, arXiv:1202.2030 [nucl-th].
- [42] A. Cieply, E. Friedman, A. Gal, D. Gazda and J. Mares, Phys. Lett. B **702**, 402 (2011).
- [43] A. Cieply, E. Friedman, A. Gal, D. Gazda and J. Mares, Phys. Rev. C **84**, 045206 (2011).
- [44] E. Friedman and A. Gal, Nucl. Phys. A **881**, 150 (2012).
- [45] D. Gazda and J. Mares, Nucl. Phys. A **881**, 159 (2012).
- [46] M. Agnello *et al.* [FINUDA Collaboration], Phys. Rev. Lett. **94**, 212303 (2005).
- [47] M. Agnello *et al.* [FINUDA Collaboration], Phys. Lett. B **654**, 80 (2007).
- [48] T. Suzuki *et al.* [KEK-PS E549 Collaboration], Phys. Rev. C **76**, 068202 (2007).
- [49] E. Oset and H. Toki, Phys. Rev. C **74**, 015207 (2006).
- [50] V. K. Magas, E. Oset, A. Ramos and H. Toki, Phys. Rev. C **74**, 025206 (2006).
- [51] V. K. Magas, E. Oset and A. Ramos, Phys. Rev. C **77**, 065210 (2008).
- [52] N. Kaiser, P. B. Siegel and W. Weise, Nucl. Phys. A **594**, 325 (1995).
- [53] E. Oset and A. Ramos, Nucl. Phys. A **635**, 99 (1998).
- [54] J. A. Oller and U. G. Meissner, Phys. Lett. B **500**, 263 (2001).
- [55] M. F. M. Lutz and E. E. Kolomeitsev, Nucl. Phys. A **700**, 193 (2002).
- [56] E. Oset, A. Ramos and C. Bennhold, Phys. Lett. B **527**, 99 (2002) [Erratum-ibid. B **530**, 260 (2002)].
- [57] D. Jido, J. A. Oller, E. Oset, A. Ramos and U. G. Meissner, Nucl. Phys. A **725**, 181 (2003).
- [58] T. Sekihara, D. Jido and Y. Kanada-En'yo, Phys. Rev. C **79**, 062201 (2009).
- [59] O. Braun, H. J. Grimm, V. Hepp, H. Strobele, C. Thol, T. J. Thouw, D. Capps and F. Gandini *et al.*, Nucl. Phys. B **129**, 1 (1977).
- [60] D. Jido, E. Oset and T. Sekihara, Eur. Phys. J. A **42**, 257 (2009).
- [61] T. Sekihara, T. Hyodo and D. Jido, Phys. Rev. C **83**, 055202 (2011).
- [62] E. Oset and W. Weise, Nucl. Phys. A **319**, 477 (1979).
- [63] D. Jido, E. Oset and J. E. Palomar, Nucl. Phys. A **694**, 525 (2001).
- [64] T. Sekihara, J. Yamagata-Sekihara, D. Jido and Y. Kanada-En'yo, in preparation.
- [65] J. Yamagata, H. Nagahiro, Y. Okumura and S. Hirenzaki, Prog. Theor. Phys. **114**, 301 (2005) [Erratum-ibid. **114**, 905 (2005)].
- [66] J. Yamagata and S. Hirenzaki, Eur. Phys. J. A **31**, 255 (2007).
- [67] J. Yamagata-Sekihara, talk at HYP2012 – XI International Conference on Hypernuclear and Strange Particle Physics.
- [68] E. Oset and A. Ramos, Nucl. Phys. A **679**, 616 (2001).
- [69] W. Weise and R. Hartle, Nucl. Phys. A **804**, 173 (2008).
- [70] J. Yamagata-Sekihara, D. Jido, H. Nagahiro and S. Hirenzaki, Phys. Rev. C **80**, 045204 (2009).